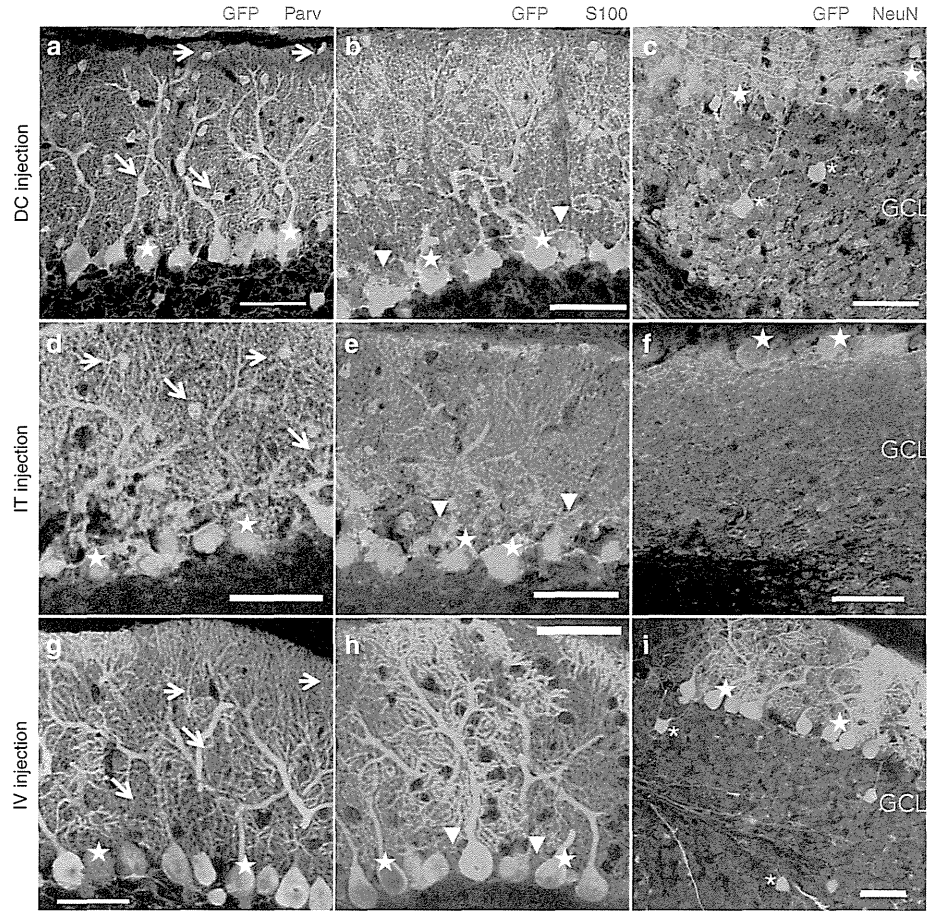

Figure 5 Cell types transduced in the cerebellar cortex after each of the three different administration routes. Slices were double-immunolabeled for GFP and parvalbumin (Parv) (left images), S100 (middle images), or NeuN (right images). (**a**–**c**) Sections from the mice treated with DC injections. (**d**–**f**) Sections from the mice treated with IT injections. (**g**–**i**) Sections from the mice treated with IV injections. Short and long arrows indicate stellate cells and basket cells, respectively. Stars and arrowheads indicate PCs and Bergmann glia, respectively. Golgi cells are marked by asterisks. GCL, granule cell layer. Scale bars, 50 μm.

among the three groups during the observation period (Figure 7c), suggesting that the poor rotarod performance was not due to the maldevelopment of ATXN1-expressing mice.

Significant atrophy of the PC dendrites 2 months after the DC injection of the ssAAV9 vectors expressing mutant ATXN1

The cerebella of ssAAV9-treated and PBS-injected control mice were examined by triple immunostaining with anti-calbindin, anti-HA and anti-expanded polyglutamine (clone 1C2) antibodies 8 weeks after the injection. The cerebellar cortices of PBS-injected mice and mice treated with ssAAV9 vectors expressing GFP showed homogenous immunolabeling for calbindin (Figure 8b,c,e,f), whereas inhomogeneous reduced immunostaining of the cerebellar cortex was observed in the cerebella treated with ssAAV9 vectors expressing ATXN1(Q141) (Figure 8a,d). A quantitative analysis showed that the immunostaining for calbindin was significantly decreased in the cerebellar cortices expressing mutant ATXN1(Q141), but not in those expressing GFP (Figure 8m). These findings suggest a decrease in the levels of calbindin in the mutant ATXN1-expressing PCs as reported in conventionally generated SCA1 mouse models expressing ATXN1(Q82) in PCs.[19,20]

In the enlarged image of the cerebellar cortex expressing ATXN1(Q141), we observed 1C2-positive mutant ATXN1 aggregates in the PC nuclei (Figure 8g) and an aberrant dendrite morphology of the PCs, such as double or triple primary dendrites (Figure 8h,i, arrows), markedly decreased branching and reduced dendritic area (Figure 8d). These changes were not detected in the cerebellar cortex treated with ssAAV9 vectors expressing GFP or with PBS (Figure 8e,f). The extent of PC dendrite atrophy was quantitatively assessed by the molecular layer thickness. The molecular layer thickness of the cerebella in the three groups was evaluated at lobule 6 because it was uniformly degenerated in the mutant ATXN1 group as judged by the decreased immunoreactivity for calbindin. The thickness, which was measured according to a protocol used by Furrer *et al.*[21] using six mice per group, was significantly decreased in the mice treated with ssAAV9 vectors expressing ATXN1(Q141) (70.8 ± 2.0 μm, $^{***}P < 0.001$) compared with the PBS-injected control mice (119.2 ± 2.2 μm) and the mice treated with ssAAV9 vectors expressing GFP (120.9 ± 4.4 μm) (Figure 8j,k,l,n). Because the intranuclear aggregation of mutant protein, a decreased immunoreactivity for calbindin, an aberrant PC dendrite morphology and a decrease in the molecular layer thickness were characteristic of conventional SCA1 mouse models,[19,20] the present results indicate that a SCA1 mouse model can be reliably generated by the DC injection of a ssAAV9 vector expressing mutant ATXN1.

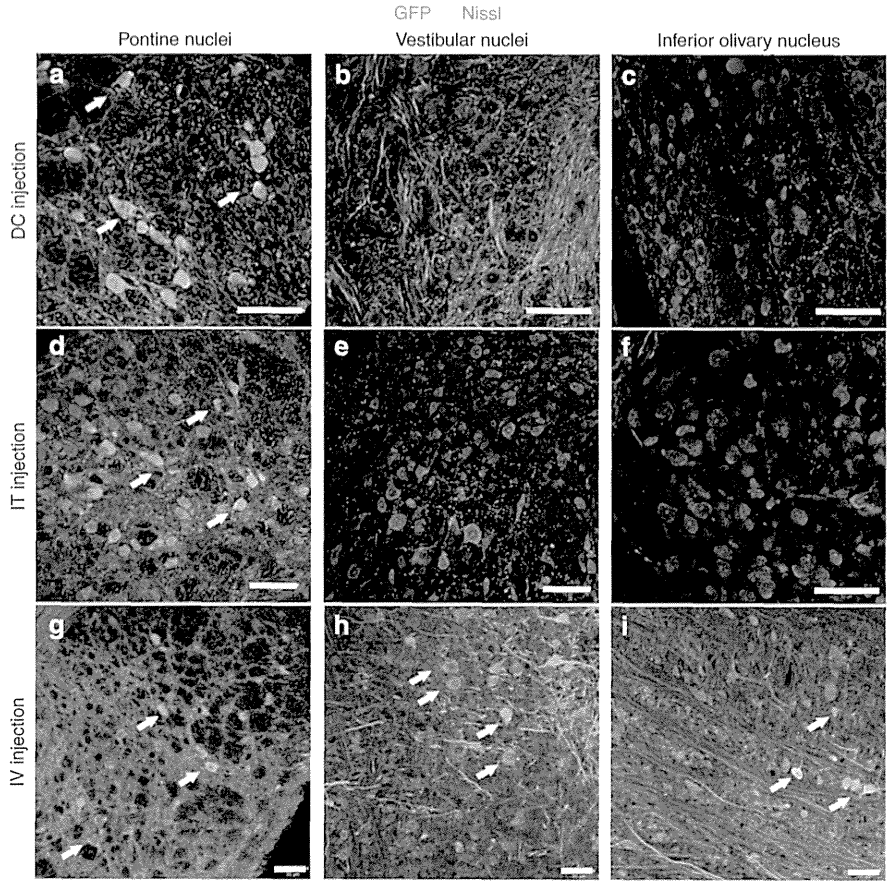

Figure 6 Transduction of neurons in the brainstem nuclei associated with the cerebellar cortex due to the three routes of administration. Sections of the brainstem were double-immunolabeled for GFP (green) and Nissl substance (red). The left, middle and right images show the pontine nuclei, vestibular nuclei and inferior olivary nucleus, respectively. (**a**–**c**) Sections from the mice that received DC injections. (**d**–**f**) Sections from the mice that received IT injections. (**g**–**i**) Sections from the mice that received IV injections. Some GFP-expressing neurons are highlighted by arrows. Scale bars, 50 μm.

DISCUSSION

Distinct transduction area and strength by three different injection routes

The route of administration of viral vectors is a critical factor that determines the tissues/organs transduced, the strength of the targeted transgene expression and the risk of tissue damage inherent to the injection procedure. However, there has been no report that directly compares DC, IT, and IV routes using the same AAV vector construct. In the present study, we compared these three administration routes and showed that the most invasive route, DC injection, resulted in a strong and diffuse transgene expression that was almost exclusively limited to the cerebellum. The next most invasive route (IT), which released vectors into the cisterna magna, caused a broad transgene expression in areas including the cerebrum, the brainstem and, most efficiently, the spinal cord; however, this route of administration only transduced a limited part of the cerebellum (lobules 9–10) near the injection site. Interestingly, we observed GFP expression in the olfactory bulb by the IT route (Figure 2f), which presumably occurred because of the combined effects of gravitation and cerebrospinal fluid flow on the viral vector spread. By contrast, the least invasive route of administration (IV injection) produced a relatively weak expression of the transgene, but the expression spanned the entire CNS.

Non-selective neuronal transduction by DC or IT injection and PC-predominant transduction through the IV route

In terms of the types of cells transduced in the cerebellum, there was no difference between the DC and IT injection routes; ssAAV9 vectors administered via either injection route transduced nearly all neuron types present in the cerebellum. By contrast, IV administration resulted in a selective transduction of PCs and projection neurons in the DCN and a small number of Golgi cells.[16] There are at least three possible explanations for the differences in the types of neurons transduced by the DC and IT injection routes and the IV injection route. First, the PC-selective transduction through the IV route might be influenced by the low viral vector dose and the detection limit.[22] A higher dose of viral vectors might increase transduction in various cell types, and more sensitive optical devices might be able to detect weaker transgene expression. Second, the difference in the ages of the mice that received ssAAV9 vectors via the DC and IT injection routes or via the IV injection route may account for the difference.[23] The morphologies and the localizations of the cortical neurons in the cerebellum differ according to the maturity; therefore, it would not be surprising if the tropism of the ssAAV9 for cortical cells differs depending on the age of the mouse.[24,25] Third, the immunity and the metabolism of the circulating blood may have affected the viral tropism. When viral vectors are injected via the IV route, they are subject to interact with immune factors and/or to

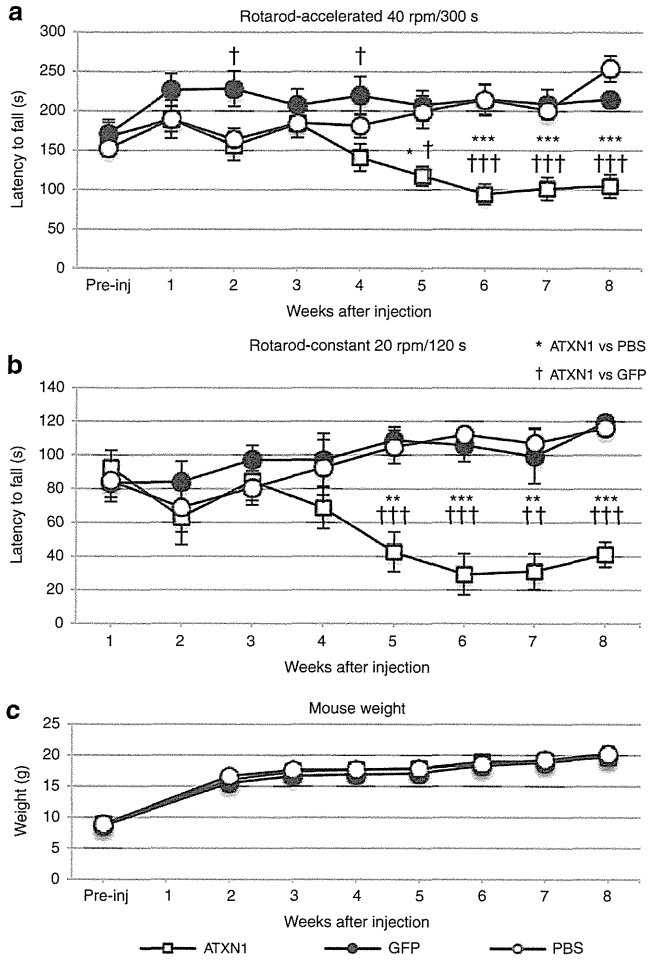

Figure 7 Progressive behavioral impairment in mice that received DC injection of ssAAV9 vectors expressing ATXN1(Q141). Four-week-old C57BL/6 mice received an injection of phosphate-buffered saline (PBS) or ssAAV9 vectors expressing ATXN1(Q141) or GFP. (**a**,**b**) The motor coordination of the mice was tested with a rotating rod. Mice underwent four trials per day on both the accelerating (**a**) (4–40 rpm) rotarod and subsequently the constant (**b**) (20 rpm) rotarod immediately before and every week up to 8 weeks after the injection. The rotarod performances of the mice expressing mutant ATXN1 ($n = 6$ mice) were compared with those of the mice treated with PBS ($n = 6$) or the mice expressing GFP ($n = 6$). (**c**) Body weights of mice from the three experimental groups. Asterisks and daggers indicate statistically significant differences compared with the PBS-injected mice and the mice injected with ssAAV9 vectors expressing GFP, respectively, as determined by one-way analysis of variance followed by Tukey's *post hoc* test, $^{*}P < 0.05$, $^{**}P < 0.01$, $^{***}P < 0.001$, $^{\dagger\dagger}P < 0.01$, and $^{\dagger\dagger\dagger}P < 0.001$.

receive modifications of the surface molecules by proteases, which could eventually alter the viral tropism.

Generation of a SCA1 mouse model by the DC injection of ssAAV9 vectors

Previously, de Almeida's group has reported lentiviral vector-mediated expression of Mutant *Huntingtin*, a gene responsible for Huntington disease[26] or mutant *ATXN3*, a gene responsible for SCA3,[27] in the rat striatum. The injected animals showed neuropathology characteristic of the diseases including intranuclear inclusions and neuronal cell death. However, those animals failed to show

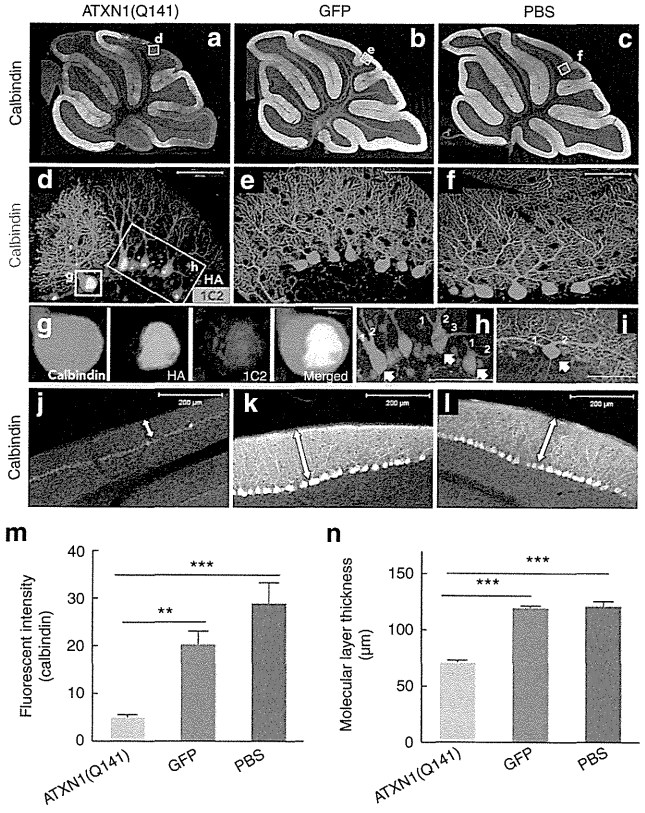

Figure 8 Neurodegenerative changes in the cerebellar cortex following the DC injection of ssAAV9 vectors expressing mutant ATXN1. (**a**–**c**) Sagittal section of the cerebellum of mice that received DC injection of (**a**) ssAAV9 vectors expressing ATXN1(Q141), (**b**) ssAAV9 expressing GFP or only (**c**) PBS. The sections were immunolabeled for calbindin. Note that calbindin immunoreactivity was diffusely decreased only in a section expressing mutant ATXN1(Q141), which is a finding characteristic of PC degeneration. (**d**–**f**) Impairment of PC dendrites after DC injection of the ssAAV9 vectors expressing mutant ATXN1. Cerebellar sections from the mice treated with the (**d**) ssAAV9 vectors expressing mutant ATXN1(Q141) were triple immunolabeled for calbindin (red), HA-tagged with mutant ATXN1 (green) and abnormally expanded polyglutamine (blue). Sections from the mice treated with (**f**) PBS or (**e**) ssAAV9 vectors expressing GFP were immunolabeled for calbindin. (**d**) PCs expressing mutant ATXN1, but not (**e**) PCs expressing GFP or (**f**) PBS-treated PCs, show aberrant dendritic morphology, such as two or more primary dendrites and markedly reduced branching. (**g**) An enlarged image of the PC soma in **d** shows nuclear localization of the mutant ATXN1 immunostained for HA, which was coimmunolabeled for abnormally expanded polyglutamine (1C2 immunostaining). (**h**,**i**) Aberrant multiple primary dendrites of PCs expressing mutant ATXN1(Q141). Arrows indicate PCs with double or triple primary dendrites as numbering. (**j**–**l**) Significant decrease in the immunoreactivity for calbindin and thickness of the molecular layer from the mice that received DC injection of the ssAAV9 vectors expressing ATXN1(Q141). Bidirectional arrows show the molecular layer of the lobule 6. (**m**) Significant decrease in the fluorescent intensity of calbindin in PCs by expression of mutant ATXN1. Graph shows the fluorescent intensity of calbindin, which were measured in the molecular and PC layers of the cerebellar lobule 6 from mice treated with ssAAV9 vectors expressing ATXN1(Q141), (**b**) ssAAV9 expressing GFP or only (**c**) PBS. (**n**) Quantitative analysis of the molecular layer thickness. The molecular layer thickness was measured as previously described by Furrer *et al.*[21] at every 200 μm in lobule 6 using three to four sections/mouse (six mice in each group). The molecular layer thickness was significantly decreased only in the mice treated with the ssAAV9 vectors expressing mutant ATXN1. Scale bars, (**d**–**f**,**h**,**j**) 50 μm and (**j**–**l**) 200 μm. Asterisks indicate statistically significant differences determined by one-way analysis of variance followed by Tukey's *post hoc* test, $^{**}P < 0.01$, $^{***}P < 0.001$.

progressive ataxia, probably because the areas of transgene expression by lentiviral vectors were spatially limited. In this study, we used diffusible ssAAV9 vectors, whose diameters are much smaller than those of lentiviral vectors, for expression of mutant ATXN1 in the cerebellum. As discussed above, a robust transgene expression in the whole cerebellum can be attained by the DC injection of ssAAV9 vectors. Therefore, we chose the DC injection of ssAAV9 vectors for expression of the disease-causing gene. Injection of ssAAV9 vectors containing mutant ATXN1 via the DC injection route caused a progressive motor deficit, which started at 5 weeks after injection. In the immunohistochemistry studies, we observed 1C2-immunolabeled mutant ATXN1 in the PC nuclei, a reduced calbindin immunostaining, an atrophy of the PC dendrites and a decrease in the molecular layer thickness. These findings are characteristic of the conventional SCA1 mouse models.[19,20,28,29] Collectively, in terms of the use of AAV vectors and demonstration of progressive ataxia, our viral vector-based SCA1 model mouse is quite new and provides an alternative strategy for generation of disease model animals.

Here, we used the DC injection route to express a mutant gene in the cerebellum, but the IT injection route is available to express a transgene in neurons of the spinal cord. Moreover, the combination of the DC injection route with the IT injection route allows us to express a mutant gene strongly throughout the CNS, which may be useful to generate animal models of disease in which broad CNS regions are affected, such as the diffuse types of the SCAs.

We examined the behavioral phenotype of mice virally expressing mutant SCA gene for longer time and found that those mice continued to show poor rotarod performance stably during our observation period (~6 months, data not shown), consistent with previous studies demonstrating long-lasting and stable expression of a transgene by AAV vectors.[30–32] Thus, our AAV-based SCA mouse model may be available also for a long-term study such as monitoring the effect of a therapeutic intervention on the ataxic behavior.

Advantages and disadvantages of the IV injection route

A big advantage of the IV injection route is an absence of the needle track damage in the brain tissue, which leads the adverse immune response via migration of microglia, in addition to the physical destruction of the neural tissue. Since the DC injection route, which was found to cause high levels of transgene expression, has a potential risk of inducing the endoplasmic reticulum stress in transduced cells, widespread low levels of transgene expression by the IV route may be safe and good for gene therapy.

One concern in systemically applying ssAAV9 vectors to target the CNS is the transduction of non-CNS organs. We examined several internal organs and the skeletal muscle of mice that received ssAAV9 vectors by the IV injection route. In accordance with the results of other groups,[12,13] we observed a faint, but apparent, GFP expression, particularly in the liver and heart (data not shown), although we used a neuron-specific modified synapsin I promoter.[33] Therefore, it would be a challenge to find a method or a promoter that transduces only the CNS.

Another disadvantage of the IV injection route is the failure of gene delivery with ssAAV vectors to the neurons of mature animals,[12] which is most likely due to the development of the blood-brain barrier. Therefore, we used P1 pups to examine the transduction profile in the CNS after an IV injection of ssAAV9 vectors. Although the expression levels of the transgene after an IV injection were fairly low, we have previously confirmed that such low levels of transgene expression are functionally effective in facilitating the degradation of toxic polyglutamine protein in the PCs of a SCA3 animal model.[34] Thus, the IV injection route could potentially be applied in newborn infants who are diagnosed with mucopolysaccharidosis during newborn screening. In such cases, the IV injection of ssAAV9 vectors expressing a deficient enzyme may help degrade the mucopolysaccharides that would otherwise accumulate and produce adverse effects in the brain. Intriguingly, scAAV transduced the CNS after a systemic injection until 3 years of age in the cynomolgus macaque,[35] suggesting that the differences in the species and/or the genomic structure of AAV broadens the transduction window of the IV injection route to target the CNS.

Perspective of AAV vectors

Here, we demonstrated that the use of different ages of mice and different routes of administration to deliver ssAAV9 vectors resulted in distinct transgene expression profiles in the CNS. Moreover, the expression levels attained by the DC injection route were sufficient to induce a characteristic behavioral phenotype and pathological alteration in the infected neurons. Therefore, we believe that in addition to exploring the functions of unknown genes in the CNS, AAV vectors are increasingly used for the generation of animal models of neurological diseases and preclinical/clinical trials of gene therapy that aim to deliver a therapeutic gene to the affected CNS regions.

MATERIALS AND METHODS

Animals

Animals were maintained on a 12-hour light/dark cycle with free access to food and water. All animal experiments were approved by the Animal Care and Experimental Committee of Gunma University (Gunma, Japan) (09-020) and were conducted in accordance with the institutional and national guides for the care and use of laboratory animals. All efforts were made to minimize animal suffering and reduce the number of animals used.

Production of ssAAV9 vectors

Recombinant ssAAV9 vectors were generated by the co-transfection of 293T cells with three plasmids, including pAAV/Syn1mCMV-GFP-WPRE or pAAV/Syn1mCMV-HA-ATXN1(Q141)-WPRE, pHelper (Stratagene, La Jolla, CA) and pAAV2/9 (kindly provided by James M Wilson of University of Pennsylvania). The viral particles were purified using ammonium sulfate precipitation and iodixanol continuous gradient centrifugation as described previously.[36] The genomic titer of the purified ssAAV9 vector as determined by real-time PCR was 7.1×10^{13} – 3.2×10^{14} vector genomes (vg)/ml.

Direct cortical injection

The ssAAV9 vector solution was injected as described previously.[16,37] Briefly, 4-week-old mice were anesthetized via an intra-peritoneal injection of ketamine (100 mg/kg weight) and xylazine (16 mg/kg weight). After a sufficient anesthesia level was attained, the mouse was mounted in a stereotactic frame, the skin on the mouse's head was cut, and a burr-hole was made in the occipital bone 5 mm caudal to bregma. Then, the blunt-ended tip of a Hamilton syringe (33 gauge) attached to a micropump (UltramicroPump II; World Precision Instrument (WPI) Sarasota, FL) was placed below the pia mater at lobule 6 (Figure 1b,c). Ten microliters of ssAAV9 vector solution expressing GFP (titer: 7.1×10^{10} vg; 5×10^{9} vg for control experiments of mouse model generation), ssAAV9 vectors expressing mutant ATXN1 (titer: 5×10^{9} vg) or PBS was injected at a rate of 333 nl/minute (for 30 minutes) using a microprocessor-based controller (Micro4; WPI, Sarasota, FL). After suturing the scalp, the mouse was maintained on a heating pad and then returned to a standard cage.

Intrathecal injection

The mice were anesthetized with a mixture of ketamine and xylazine similar to that used for DC injection and then fixed in a stereotactic frame. For the injection of ssAAV9 vectors into the cisterna magna, the skin over the posterior atlanto-occipital membrane was cut, and the muscular layers

were moved aside. The tip of a Hamilton syringe (30 or 33 gauge) was carefully inserted into the cisterna magna through the posterior atlanto-occipital membrane, and the ssAAV9 vector was introduced as depicted in Figure 1b,c. Similar to DC injection, 10 microliters of ssAAV9 vector solution containing 7.1×10^{10} vg was injected. The muscular layers and skin were closed by suture, and the mouse was kept on a heating pad and returned to the standard cage after it recovered from anesthesia.

Intravenous injection

The ssAAV9 vector solution was injected into the temporal superficial vein as illustrated in Figure 1b,d. One-day-old pups that weighed about 1.6 g were anesthetized by hypothermia on a latex covered petri-dish inside a Styrofoam box containing ice for 2–4 minutes. Then, the mice were positioned by hand to reveal the superficial temporal vein. The ssAAV9 vector solution (titer: 4.4×10^{11} vg/g) was administered via the superficial-temporal vein using a 30-gauge insulin syringe as described by Foust *et al.*[23]

Immunohistochemistry

Mice were perfused transcardially with a fixative containing 4% paraformaldehyde in 0.1 mol/l PBS after being deeply anesthetized with ketamine/xylazine. The whole brain was removed and postfixed in the same fixative overnight. Sagittal and transverse sections were produced from the cerebellar vermis and the whole cerebellum, respectively, using a vibratome/microtome (Leica VT1000 S; Leica Microsystems, Wetzlar, Germany). The cerebellar sections were placed in a blocking solution, which contained 2% normal donkey serum and 0.4% Triton X-100 in PBS, for 1 hour. To evaluate the levels and expansion of GFP expression in the cerebellum, the cerebellar sections were immunolabeled for GFP and Nissl substance (Figure 3a,c,e,g) or calbindin (Figure 3b,d,f,h). For the primary antibody treatment, the sections were incubated with rat polyclonal anti-GFP (1:1,000; Cat. No. GF090R, Nacalai tesque, Kyoto, Japan) and mouse monoclonal anti-calbindin D-28K (1:500; Cat. No. 300, Swant, Bellinzona, Switzerland) antibodies overnight at 4 °C on a shaking table. After washing with PBS at room temperature (5 minutes × 3 times), the sections were treated with Neurotrace530/615 (1:250; Life Technologies, NY) and/or secondary antibodies in the blocking solution at room temperature for 4 hours. The secondary antibodies included Alexa Fluor 488-conjugated donkey anti-rat IgG (1:500; Life Technologies) and Alexa Fluor 568-conjugated donkey anti-mouse IgG (1:500; Life Technologies).

For determining the % ratio of the transduced PCs to the whole PCs, the cerebellar sections were immunolabeled for GFP and Nissl substance or calbindin (Figure 4) as described above. To identify the transduced cell types, the cerebellar sections were immunolabeled for GFP and parvalbumin, S100 or NeuN (Figure 5). The primary antibodies included rat polyclonal anti-GFP (1:1,000; Cat. No. GF090R, Nacalai tesque) and mouse monoclonal anti-parvalbumin (1:500; Cat. No. P3088, Sigma-Aldrich, St Louis, MO), mouse monoclonal anti-S100 (1:500; Cat. No. S2532, Sigma-Aldrich) or mouse monoclonal anti-neuron-specific nuclear protein (NeuN; Cat. No. MAB377; Millipore, Billerica, MA) antibodies. The secondary antibodies included Alexa Fluor 488-conjugated donkey anti-rat IgG (1:500; Life Technologies) and Alexa Fluor 568-conjugated donkey anti-mouse IgG (1:500; Life Technologies). Transduction of the brain stem was assessed by immunolabeling the brain stem sections for GFP and Nissl substance (Figure 6) as described above.

The expression of the mutant ATXN1 in the PCs was visualized by immunolabeling for calbindin and HA tagged with the ATXN1. An abnormally expanded polyglutamine stretch involved in the mutant ATXN1 was also detected by the monoclonal antibody (clone; 1C2). Thus, the cerebellar sections expressing mutant ATXN1 (Figure 8a,d,g,h) were triple immunostained with rabbit polyclonal anti-calbindin (1:500; Cat. No. C2724, Sigma-Aldrich), rat monoclonal anti-HA (1:500, Cat. No. 11867423001, Roche, IN) and mouse monoclonal anti-expanded polyglutamine (1:500, clone, 1C2, Cat. No. MAB1574, Millipore) antibodies, whereas the cerebellar sections from the control mice (Figure 8b,c,e,f,i,j) were single immunolabeled with rabbit polyclonal anti-calbindin (1:500; Cat. No. C2724, Sigma-Aldrich). For the sections that were immunostained by 1C2, to maximize the optimal exposure to buried 1C2 epitope, Formic Acid (98%) was applied following Osmand *et al.*[28] (with modifications) for 20 seconds before the pretreatment by blocking solution. The secondary antibodies included Alexa Fluor 568-conjugated donkey anti-rabbit IgG (1:500; Life Technologies), Alexa Fluor 488-conjugated donkey anti-rat IgG (1:500; Life Technologies), and Alexa Fluor 680-conjugated donkey anti-mouse IgG (1:500; Life Technologies).

Bright-field and fluorescent images of the whole brains and spinal cords of the mice were captured using a fluorescent stereoscopic microscope (VB-7010, Keyence, Osaka, Japan). Images of the whole brain sections were obtained using a fluorescent microscope (BZ-9000; Keyence). Images of the cerebellar sections were obtained using a confocal laser-scanning microscope (LSM 5 PASCAL; Carl Zeiss, Oberkochen, Germany).

Transduction efficacy of PCs in the cerebellum

The difference of PC transduction efficiency in the three injection routes was examined in four classified lobular regions (lobules 1–3, 4–5, 6–8, and 9–10). Serial z-stack images were obtained from 15 designated locations on a sagittal section of the cerebellum immunolabeled for GFP and calbindin. Each cerebellar lobule was represented by one or more locations. Serial z-stack images consisting of 10 images (interval: 3 μm) were captured by a confocal microscope (LSM 510, Carl Zeiss) with a 20× objective that covers a 450 μm × 450 μm area. Cell counting was performed using the free software ImageJ (National Institute of Health, Bethesda, MD) using a "Cell counter" plugin. We first counted the calbindin-positive PCs and then the GFP-positive cells that concurred with calbindin. We carefully examined the serial images from different depths to ensure that all positive cells were counted and no cell was counted more than once. Truncated cells on the image margin were counted if they were located in the right and lower margins, but were ignored if they were located in the upper and left margins. We collected 15 locations/section, 3 sections/mouse and 3 mice/group, and thus determined the PC transduction efficiency in the four classified lobular regions of the cerebellum using 135 z-stack serial images/group. The transduction efficacy of the PCs was calculated by dividing the number of GFP and calbindin-double positive PCs by the calbindin-positive PCs. The data were then averaged in the four lobular groups.

Quantification of the fluorescent intensity of GFP and calbindin

To measure the GFP fluorescent intensity, nine sections from three mice (three sections/mouse) from each route were randomly selected. The GFP fluorescent images of those sections were captured using the same setting by a confocal microscope and then analyzed using ImageJ. The outline of the cerebellar lobular groups in each section was traced, and the fluorescence intensity in the enclosed areas was measured. The background intensity was subtracted from the fluorescence intensity. For examining the immunofluorescent intensity of calbindin, 24 sections from six mice (four sections/mouse) from each group were randomly selected and the fluorescence intensity in the lobule 6 was measured as described above.

Rotarod test for motor coordination and weight measurements in mice

The motor coordination ability was assessed using a rotarod (MK-610, Muromachi Kikai, Tokyo, Japan) with two different paradigms. In the accelerated paradigm, the rod accelerated from 4 rpm to 40 rpm in 300 seconds (cut off time = 300 seconds), while in the stable speed paradigm, the rod rotated at a stable speed of 20 rpm (cut off time = 120 seconds). Mice were assessed with both paradigms immediately before (only accelerated paradigm) and every week up to 8 weeks after the viral injection. In the accelerating and stably rotating tests, the mice were subjected to four trials each, with a 30 and 15 minutes rest, respectively, between the trials. The average latency to fall from the rod was examined. Changes in the body weight were measured by decigram precision every week. Six mice were examined in each group.

Molecular layer thickness

The thickness of the molecular layer was measured as previously described by Furrer *et al.*[21] with some modifications. The molecular layer thickness was measured at every 200 μm in lobule 6 using three to four sections/mouse with a LSM Image browser (4.2 Service Pack 1, Carl Zeiss). Six mice were examined in each group.

Statistical analysis

Significant differences were analyzed by Tukey's *post hoc* test after one-way analysis of variance using the R software statistical package (www.r-project.org). Data are expressed as the means ± SEM.

CONFLICT OF INTEREST

The authors declare no conflict of interest.

ACKNOWLEDGMENTS

The authors thank our laboratory members for excellent technical assistance and constructive discussion, and James M. Wilson of the University of Pennsylvania for providing the pAAV2/9 vector for ssAAV9 production. This work was funded, in part, by the Funding Program for the Next Generation World-Leading Researchers (LS021) to H.H. and the Brain Science Program of the National Institutes of Natural Science (NINS) to A.K.

REFERENCES

1 Cavanagh, JB, Holton, JL and Nolan, CC (1997). Selective damage to the cerebellar vermis in chronic alcoholism: a contribution from neurotoxicology to an old problem of selective vulnerability. *Neuropathol Appl Neurobiol* **23**: 355–363.
2 Seidel, K, Siswanto, S, Brunt, ER, den Dunnen, W, Korf, HW and Rüb, U (2012). Brain pathology of spinocerebellar ataxias. *Acta Neuropathol* **124**: 1–21.
3 Mellon, SH, Gong, W and Schonemann, MD (2008). Endogenous and synthetic neurosteroids in treatment of Niemann-Pick Type C disease. *Brain Res Rev* **57**: 410–420.
4 Sarna, JR and Hawkes, R (2003). Patterned Purkinje cell death in the cerebellum. *Prog Neurobiol* **70**: 473–507.
5 Hirai, H (2012). Basic research on cerebellar gene therapy using lentiviral vectors. *Cerebellum* **11**: 443–445.
6 Torashima, T, Koyama, C, Iizuka, A, Mitsumura, K, Takayama, K, Yanagi, S *et al.* (2008). Lentivector-mediated rescue from cerebellar ataxia in a mouse model of spinocerebellar ataxia. *EMBO Rep* **9**: 393–399.
7 Rodriguez-Lebron, E, Denovan-Wright, EM, Nash, K, Lewin, AS and Mandel, RJ (2005). Intrastriatal rAAV-mediated delivery of anti-huntingtin shRNAs induces partial reversal of disease progression in R6/1 Huntington's disease transgenic mice. *Mol Ther* **12**: 618–633.
8 Xia, H, Mao, Q, Eliason, SL, Harper, SQ, Martins, IH, Orr, HT *et al.* (2004). RNAi suppresses polyglutamine-induced neurodegeneration in a model of spinocerebellar ataxia. *Nat Med* **10**: 816–820.
9 Qin, Q, Inatome, R, Hotta, A, Kojima, M, Yamamura, H, Hirai, H *et al.* (2006). A novel GTPase, CRAG, mediates promyelocytic leukemia protein-associated nuclear body formation and degradation of expanded polyglutamine protein. *J Cell Biol* **172**: 497–504.
10 Miller, VM, Nelson, RF, Gouvion, CM, Williams, A, Rodriguez-Lebron, E, Harper, SQ *et al.* (2005). CHIP suppresses polyglutamine aggregation and toxicity *in vitro* and in vivo. *J Neurosci* **25**: 9152–9161.
11 Lee, Y, Samaco, RC, Gatchel, JR, Thaller, C, Orr, HT and Zoghbi, HY (2008). miR-19, miR-101 and miR-130 co-regulate ATXN1 levels to potentially modulate SCA1 pathogenesis. *Nat Neurosci* **11**: 1137–1139.
12 Miyake, N, Miyake, K, Yamamoto, M, Hirai, Y and Shimada, T (2011). Global gene transfer into the CNS across the BBB after neonatal systemic delivery of single-stranded AAV vectors. *Brain Res* **1389**: 19–26.
13 Wang, DB, Dayton, RD, Henning, PP, Cain, CD, Zhao, LR, Schrott, LM *et al.* (2010). Expansive gene transfer in the rat CNS rapidly produces amyotrophic lateral sclerosis relevant sequelae when TDP-43 is overexpressed. *Mol Ther* **18**: 2064–2074.
14 McCarty, DM (2008). Self-complementary AAV vectors; advances and applications. *Mol Ther* **16**: 1648–1656.
15 Loeb, JE, Cordier, WS, Harris, ME, Weitzman, MD and Hope, TJ (1999). Enhanced expression of transgenes from adeno-associated virus vectors with the woodchuck hepatitis virus posttranscriptional regulatory element: implications for gene therapy. *Hum Gene Ther* **10**: 2295–2305.
16 Torashima, T, Okoyama, S, Nishizaki, T and Hirai, H (2006). *In vivo* transduction of murine cerebellar Purkinje cells by HIV-derived lentiviral vectors. *Brain Res* **1082**: 11–22.
17 Neki, A, Ohishi, H, Kaneko, T, Shigemoto, R, Nakanishi, S and Mizuno, N (1996). Metabotropic glutamate receptors mGluR2 and mGluR5 are expressed in two non-overlapping populations of Golgi cells in the rat cerebellum. *Neuroscience* **75**: 815–826.
18 Geurts, FJ, Timmermans, J, Shigemoto, R and De Schutter, E (2001). Morphological and neurochemical differentiation of large granular layer interneurons in the adult rat cerebellum. *Neuroscience* **104**: 499–512.
19 Zu, T, Duvick, LA, Kaytor, MD, Berlinger, MS, Zoghbi, HY, Clark, HB *et al.* (2004). Recovery from polyglutamine-induced neurodegeneration in conditional SCA1 transgenic mice. *J Neurosci* **24**: 8853–8861.
20 Vig, PJ, Wei, J, Shao, Q, Lopez, ME, Halperin, R and Gerber, J (2012). Suppression of calbindin-D28k expression exacerbates SCA1 phenotype in a disease mouse model. *Cerebellum* **11**: 718–732.
21 Furrer, SA, Mohanachandran, MS, Waldherr, SM, Chang, C, Damian, VA, Sopher, BL *et al.* (2011). Spinocerebellar ataxia type 7 cerebellar disease requires the coordinated action of mutant ataxin-7 in neurons and glia, and displays non-cell-autonomous bergmann glia degeneration. *J Neurosci* **31**: 16269–16278.
22 Inagaki, K, Fuess, S, Storm, TA, Gibson, GA, Mctiernan, CF, Kay, MA *et al.* (2006). Robust systemic transduction with AAV9 vectors in mice: efficient global cardiac gene transfer superior to that of AAV8. *Mol Ther* **14**: 45–53.
23 Foust, KD, Nurre, E, Montgomery, CL, Hernandez, A, Chan, CM and Kaspar, BK (2009). Intravascular AAV9 preferentially targets neonatal neurons and adult astrocytes. *Nat Biotechnol* **27**: 59–65.
24 Lowenstein, PR (2009). Crossing the rubicon. *Nat Biotechnol* **27**: 42–44.
25 Saunders, NR, Joakim Ek, C and Dziegielewska, KM (2009). The neonatal blood-brain barrier is functionally effective, and immaturity does not explain differential targeting of AAV9. *Nat Biotechnol* **27**: 804–5; author reply 805.
26 de Almeida, LP, Ross, CA, Zala, D, Aebischer, P and Déglon, N (2002). Lentiviral-mediated delivery of mutant huntingtin in the striatum of rats induces a selective neuropathology modulated by polyglutamine repeat size, huntingtin expression levels, and protein length. *J Neurosci* **22**: 3473–3483.
27 Alves, S, Régulier, E, Nascimento-Ferreira, I, Hassig, R, Dufour, N, Koeppen, A *et al.* (2008). Striatal and nigral pathology in a lentiviral rat model of Machado-Joseph disease. *Hum Mol Genet* **17**: 2071–2083.
28 Osmand, AP, Berthelier, V and Wetzel, R (2006). Imaging polyglutamine deposits in brain tissue. *Meth Enzymol* **412**: 106–122.
29 Stevanin, G, Trottier, Y, Cancel, G, Dürr, A, David, G, Didierjean, O *et al.* (1996). Screening for proteins with polyglutamine expansions in autosomal dominant cerebellar ataxias. *Hum Mol Genet* **5**: 1887–1892.
30 Hadaczek, P, Eberling, JL, Pivirotto, P, Bringas, J, Forsayeth, J and Bankiewicz, KS (2010). Eight years of clinical improvement in MPTP-lesioned primates after gene therapy with AAV2-hAADC. *Mol Ther* **18**: 1458–1461.
31 Husain, T, Passini, MA, Parente, MK, Fraser, NW and Wolfe, JH (2009). Long-term AAV vector gene and protein expression in mouse brain from a small pan-cellular promoter is similar to neural cell promoters. *Gene Ther* **16**: 927–932.
32 De Wit, J, Eggers, R, Evers, R, Castrén, E and Verhaagen, J (2006). Long-term adeno-associated viral vector-mediated expression of truncated TrkB in the adult rat facial nucleus results in motor neuron degeneration. *J Neurosci* **26**: 1516–1530.
33 Matsuzaki, Y, Oue, M and Hirai, H (2014). Generation of a neurodegenerative disease mouse model using lentiviral vectors carrying an enhanced synapsin I promoter. *J Neurosci Methods* **223**: 133–143.
34 Konno, A, Shuvaev, AN, Miyake, N, Miyake, K, Iizuka, A, Matsuura, S *et al.* (2014). Mutant ataxin-3 with an abnormally expanded polyglutamine chain disrupts dendritic development and metabotropic glutamate receptor signaling in mouse cerebellar Purkinje cells. *Cerebellum* **13**: 29–41.
35 Bevan, AK, Duque, S, Foust, KD, Morales, PR, Braun, L, Schmelzer, L *et al.* (2011). Systemic gene delivery in large species for targeting spinal cord, brain, and peripheral tissues for pediatric disorders. *Mol Ther* **19**: 1971–1980.
36 Miyake, K, Miyake, N, Yamazaki, Y, Shimada, T and Hirai, Y (2012). Serotype-independent method of recombinant adeno-associated virus (AAV) vector production and purification. *J Nippon Med Sch* **79**: 394–402.
37 Goenawan, H and Hirai, H (2012). Modulation of lentiviral vector tropism in cerebellar Purkinje cells *in vivo* by a lysosomal cysteine protease cathepsin K. *J Neurovirol* **18**: 521–531.

Gene Therapy (2014), 1–8

www.nature.com/gt

ORIGINAL ARTICLE

One-year follow-up of transgene expression by integrase-defective lentiviral vectors and their therapeutic potential in spinocerebellar ataxia model mice

H Saida[1,3], Y Matsuzaki[1,3], K Takayama[1,3], A Iizuka[1], A Konno[1], S Yanagi[2] and H Hirai[1]

We examined integrase-defective lentiviral vectors (IDLVs) with a mutant (D64V) integrase in terms of their residual integration capability, the levels and duration of transgene expression and their therapeutic potential in comparison to wild-type lentiviral vectors (WTLVs) with a wild-type integrase gene. Compared with WTLVs, the IDLV-mediated proviral integration into host-cell chromosomes was approximately 1/3850 in HeLa cells and approximately 1/111 in mouse cerebellar neurons *in vivo*. At 2 months, transgene expression by IDLVs in the mouse cerebellum was comparable to that by WTLVs, but then significantly decreased. The mRNA levels at 6 and 12 months after injection in IDLV-infected cerebella were approximately 26% and 5%, respectively, of the mRNA levels in WTLV-injected cerebella. To examine the therapeutic potential, IDLVs or WTLVs expressing a molecule that enhances the ubiquitin-proteasome pathway were injected into the cerebella of spinocerebellar ataxia type 3 model mice (SCA3 mice). IDLV-injected SCA3 mice showed a significantly improved rotarod performance even at 1 year after-injection. Immunohistochemistry at 1 year after injection showed a drastic reduction of mutant aggregates in Purkinje cellsfrom IDLV-injected, as well as WTLV-injected, SCA3 mice. Our results suggest that because of the substantially reduced risk of insertional mutagenesis, IDLVs are safer and potentially effective as gene therapy vectors.

Gene Therapy advance online publication, 3 July 2014; doi:10.1038/gt.2014.60

INTRODUCTION

Lentiviral vectors enable efficient, long-lasting and stable transgene expression in both dividing and quiescent cells, including postmitotic neurons.[1,2] Therefore, they are promising as therapeutic gene transfer vectors. Efficient and sustained expression of a transgene is mediated by the insertion of a proviral genome into host-cell chromosomes.[3,4] However, the random insertion of proviruses, called 'insertional mutagenesis', may disrupt critical genes, such as tumor suppressor genes and those of protein kinases/phosphatases, which potentially causes oncogenic transformation or cell death.[5–7]

The proviral insertion into host-cell chromosomes is mediated by a viral integrase. To avoid insertional mutagenesis, integrase-defective lentiviral vectors (IDLVs) have been developed, in which mutations were introduced in the coding sequence for the integrase gene or at sites in the viral genome where the integrase attaches and mediates insertion (*att* sites).[8–14] Unintegrated provirus from IDLVs resides in the nucleus as an episomal form and expresses a transgene for at least several months in neuronal cells.[14] Thus, IDLVs are safer and promising gene therapy vectors for future clinical applications. Nonetheless, several issues remain to be clarified in IDLVs, including the amount of transgene expressed by IDLVs compared with wild-type lentiviral vectors (WTLVs); how long transgene expression continues and whether the therapeutic effect of IDLVs for gene therapy is comparable to WTLVs.

In this study, we explored the temporal change in expression levels of a transgene by IDLVs, relative to WTLVs, for up to 1 year. Moreover, the usefulness of IDLVs as gene therapy vectors was evaluated by examining the behavioral recovery of spinocerebellar ataxia type 3 model mice (SCA3 mice) after injection of IDLVs or WTLVs expressing the therapeutic protein CRAG (collapsin response mediator protein-associated molecule-associated guanosine triphosphatase).[15,16]

RESULTS

Generation of lentiviral vectors with a class I integrase mutation

We used a class I integrase mutation to generate the IDLVs expressing green fluorescent protein (GFP) or GFP-P2A-CRAG under the control of the murine stem cell virus (MSCV) promoter (Figures 1a and b). This mutation had no influence on reverse transcription, nuclear import of the preintegration complex or circularization of the viral genome in the nucleus.[8] The mutation that we used in this study consisted of a substitution of the 64th aspartic acid with valine (D64V), which is localized in the core domain of the integrase[17] (Figure 1a). The mutant integrase gene was subcloned into a lentiviral packaging plasmid, namely, pCAGkGP1R, for the production of the IDLVs.

[1]Department of Neurophysiology, Gunma University Graduate School of Medicine, Maebashi, Gunma, Japan and [2]Laboratory of Molecular Biochemistry, Graduate School of Life Sciences, Tokyo University of Pharmacy and Life Sciences, Tokyo, Japan. Correspondence: Professor H Hirai, Department of Neurophysiology, Gunma University Graduate School of Medicine, 39–22, Showa-machi 3-chome, Maebashi 371-8511 Gunma, Japan.
E-mail: hirai@gunma-u.ac.jp
[3]These authors contributed equally to this work.
Received 27 February 2014; revised 12 May 2014; accepted 27 May 2014

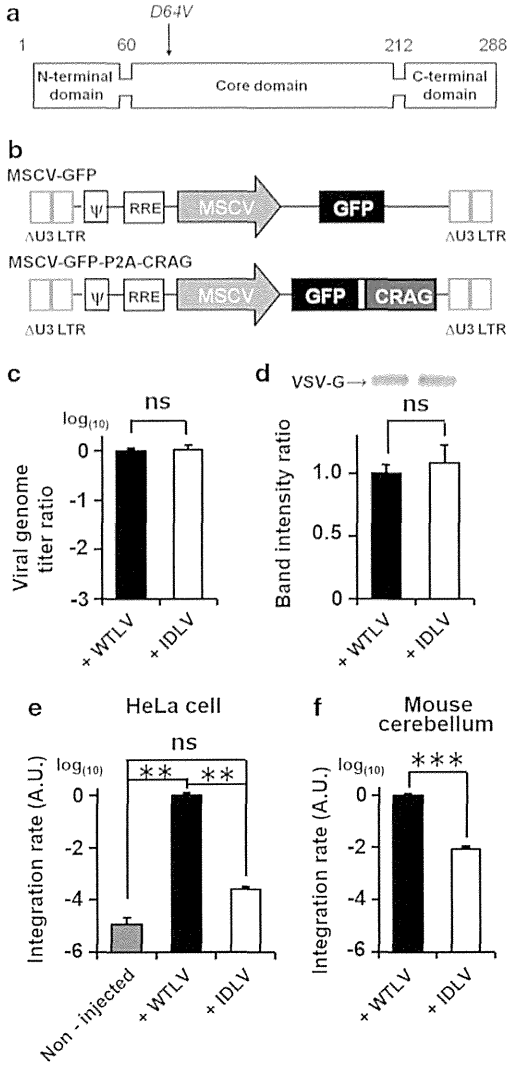

Figure 1. Significantly reduced integration of proviruses from IDLVs compared with lentiviral vectors having a wild-type integrase gene (WTLVs). (**a**) A schema showing three domains of the integrase and the relative position of the mutation (D64V) in the integrase. (**b**) Human immunodeficiency virus (HIV)-derived lentiviral vectors used in this study. The transcription of GFP or GFP-P2A-CRAG is driven by the MSCV promoter. The mRNA of GFP-P2A-CRAG is processed at the P2A sequence. Thus, CRAG is expressed separately from GFP in infected cells. U3 regions in the long-terminal repeat (LTR) were self-inactivating (ΔU3 LTR). ψ is the packaging signal, and RRE is the Rev-responsive element. (**c** and **d**) Assessment of the amounts of IDLVs and WTLVs by quantitative PCR (**c**) and western blotting (**d**). IDLVs and WTLVs (four batches each) were produced using the same protocol. Genomic titers were measured by quantitative PCR, whereas the amounts of IDLV and WTLV particles obtained from four independent cultures, respectively, were examined by western blotting using antibodies against the envelope glycoprotein VSV-G. There was no statistically significant difference (ns) between the two groups. (**e** and **f**) Drastic reduction of proviral integration by IDLVs, compared with WTLVs, in cultured HeLa cells (**e**) or mouse cerebellum *in vivo* (**f**). Proviral integration into the host chromosome was examined by real-time quantitative Alu-PCR or B1-PCR. In each group, four (**e**) or five (**f**) independent experiments were conducted. $^{**}P < 0.01$ and $^{***}P < 0.001$ by Tukey's *post hoc* test after one-way analysis of variance (ANOVA).

No influence of the integrase mutation on the production of IDLVs in HEK293T cells

To examine whether mutation in the integrase gene affected production of viral vectors, IDLVs and WTLVs were simultaneously produced using the same protocol. The genomic titers were determined by quantitative reverse transcriptase-PCR using four batches each of IDLVs and WTLVs. The genomic titers of WTLVs and IDLVs were $1.42 \pm 0.18 \times 10^{11}$ and $1.47 \pm 0.29 \times 10^{11}$ vector genomes (vg) ml^{-1}, respectively, and there was no significant difference between the two groups (Figure 1c). We also assessed the amounts of virion particles of IDLVs and WTLVs, both of which were obtained from four independent cultures by western blotting using an antibody against the envelope glycoprotein, vesicular stomatitis virus-G protein (VSV-G). The band intensities for VSV-G on the blot were comparable between WTLVs and IDLVs (Figure 1d). These results indicate that the integrase mutation did not affect the production of lentiviral vector particles in human embryonic kidney 293T (HEK293T) cells.

Drastic reduction of chromosomal integration of proviruses from IDLVs

We next examined the integration of the proviral genome derived from IDLVs or WTLVs into chromosomes of HeLa cells or mouse cerebellar cells *in vivo*. HeLa cells cultured in a 6-cm dish were infected with 1 μl of WTLVs or a same volume of IDLVs with the same titer. The cells were collected at 4 days after lentiviral infection, and real-time quantitative Alu-PCR was performed. The integration efficiency of IDLVs was significantly reduced to 1/3850 compared with WTLVs; the ratio of proviral integration by IDLVs to that by WTLVs was $2.6 \pm 0.6 \times 10^{-4}$ ($P < 0.01$, $n = 8$ culture pairs) (Figure 1e).

Then, we examined the efficiency of proviral integration by IDLVs *in vivo*. Ten μl of the IDLVs (1.47×10^{11} vg ml^{-1}) or the same volume of WTLVs (1.42×10^{11} vg ml^{-1}) that expressed GFP under the control of the MSCV promoter was injected into postnatal day (P) 27 or P28 mouse cerebellum (five mice, each). At 1 week after the viral injection, GFP-expressing cerebellar tissue was resected under a fluorescence stereoscopic microscope. Subsequently, the integrated proviral genome was quantified by real-time quantitative B1-PCR (see the Materials and Methods section). The integration efficiency of IDLVs in the cerebellum *in vivo* was significantly reduced to $< 1/100$ of WTLVs ($P < 0.001$) (Figure 1f). Thus, the D64V mutation in the integrase significantly prevented IDLVs from proviral integration into host-cell genomes in both cultured cells and the cerebellum *in vivo*.

Spatiotemporal change in the expression of GFP by IDLVs and WTLVs

We found that the efficiency of proviral integration by IDLVs in the cerebellum *in vivo* was $< 1/100$ of that by WTLVs. We next compared the spatial and temporal profiles of GFP expression by IDLVs in the cerebellum *in vivo* with those by WTLVs up to 1 year after the viral injection. Ten μl of WTLVs (1.47×10^{11} vg ml^{-1}) or the same volume of WTLVs (2.69×10^{11} vg ml^{-1}) was injected into the mouse cerebella as described in the Materials and methods section. The mice were killed at 2, 6 and 12 months after the viral injection. At 2 and 6 months after the viral injection, the gross GFP fluorescence emitted from the whole cerebella, which was detected under a fluorescence stereoscopic microscope, was approximately the same between IDLVs and WTLVs (Figures 2a, b, g and h). At 1 year after viral injection, the GFP fluorescent area on the IDLV-treated (Figure 2i), but not the fluorescent area on the WTLV-treated (Figure 2c), cerebellum was markedly decreased.

Sagittal sections of the cerebellar vermis that received injection of WTLVs or IDLVs showed GFP expression primarily in Purkinje cells (PCs) and less efficiently in interneurons in the molecular

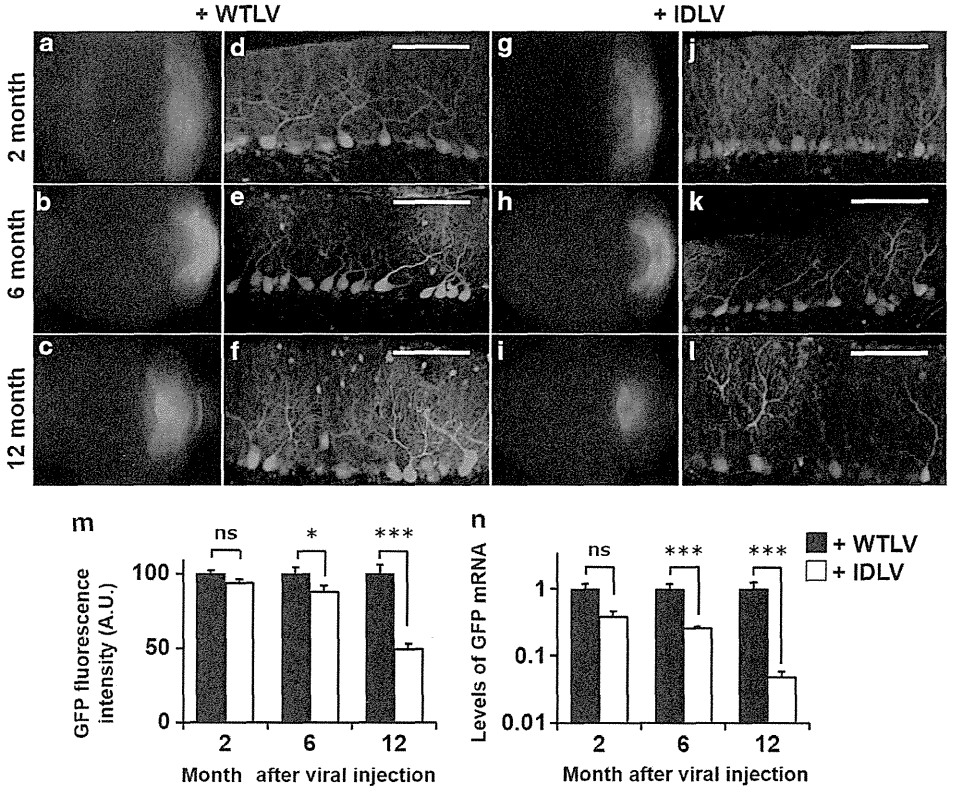

Figure 2. Temporal change in the levels of transgene expression in the cerebella injected with WTLVs or IDLVs. (**a–l**) Representative GFP fluorescence images of whole brains (**a–c** and **g–l**) and their sagittal sections of the cerebellar vermis (**d–f** and **j–l**). Mice received an injection of WTLVs expressing GFP (**a–f**) or IDLVs expressing GFP (**g–l**). GFP expression in the cerebella was examined at 2 (upper images), 6 (middle images) and 12 months (lower images) after injection. (**m**) Change in the GFP fluorescence intensity in PC somata at 2, 6 and 12 months after the viral injection. GFP fluorescence intensity in more than 100 PCs was measured from three WTLV-treated and three IDLV-treated cerebella, and the % ratio of the intensity in IDLV-infected PCs compared with that in WTLV-infected PCs was expressed. (**n**) Change in the levels of GFP mRNA in the cerebellar cortex at 2, 6 and 12 months after the viral injection. The cerebellar vermis was excised from WTLV- and IDLV-treated cerebella, and GFP mRNA was measured by quantitative PCR. The ratio of the levels of GFP mRNA in IDLV-infected tissue to those in WTLV-infected tissues was expressed. $^{*}P < 0.05$ and $^{***}P < 0.001$ by an unpaired *t*-test. ns, not significant. Scale bar, 100 μm.

layer (Figures 2d, f and j–l). Because the GFP fluorescence images of the cerebellar cortex were obtained from the efficiently transduced areas close to the viral injection site, GFP expression in PCs appears to be maintained even 12 months after the IDLVs injection (Figure 2l).

GFP fluorescence intensity in the PC somata was quantitatively examined in the cerebella treated with IDLVs or WTLVs, and the GFP fluorescence levels resulting from IDLVs were expressed as the ratio relative to those resulting from WTLVs. GFP fluorescence intensity in PCs transduced by IDLVs was approximately 93% of that observed in WTLV-transduced cells at 2 months after the injection, and there was no statistically significant difference in GFP fluorescence intensity in the PC somata between IDLV- and WTLV-treated mice. However, the GFP fluorescence intensity was significantly reduced to 87% ($P < 0.05$) and 49% ($P < 0.001$) of that by WTLVs at 6 and 12 months after the injection, respectively (Figure 2m).

The temporal change in the expression levels of GFP mRNA in IDLV-treated cerebella compared with WTLV-treated cerebella was further assessed by quantitative PCR. The cerebellar vermis was excised from IDLV- and WTLV-treated cerebella at 2, 6 and 12 months after the injection. The amount of GFP mRNA in the IDLV-treated cerebella was comparable to that in the WTLV-treated cerebella at 2 months, but significantly decreased to approximately 25% at 6 months ($P < 0.001$) and $< 5\%$ at 12 months after the viral injection ($P < 0.001$) (Figure 2n).

Restoration of rotarod performance in SCA3 mice treated with IDLVs expressing CRAG

Previously, we injected WTLVs expressing CRAG into the cerebellar cortex of ataxic SCA3 mice that expressed mutant ataxin-3 under the control of the PC-specific L7 promoter.[16] Expression of CRAG caused degradation of mutant ataxin-3 aggregates in PCs through the ubiquitin-proteasome pathway,[15] resulting in a rescue of the ataxia phenotype. Then, using this system, we examined the therapeutic efficacy of IDLVs for up to 1 year after the injection. Ten microliters of WTLVs (over 1.0×10^{10} transduction units/ml^{-1}, which corresponds roughly to 1.0×10^{11} vg ml^{-1} or higher) or IDLVs with the similar genome titer, both of which expressed GFP-P2A-CRAG, were injected into 3-week-old SCA3 mice, and the rotarod performance was examined immediately before and at 2, 6 and 12 months after the viral injection.

In the accelerating protocol (Figure 3a), untreated SCA3 mice stayed on the rod only for approximately 20 s, and the time gradually decreased to approximately 10 s at 1 year of age. The SCA3 mice that received an injection of IDLVs expressing GFP alone showed a rotarod performance approximately the same as non-injected SCA3 mice at up to 12 months after the viral injection. In contrast, a significantly better rotarod performance was observed in the SCA3 mice that received an injection of IDLVs expressing GFP-P2A-CRAG at 2 ($P < 0.05$) and 6 ($P < 0.01$) months after the viral injection compared with non-injected control SCA3

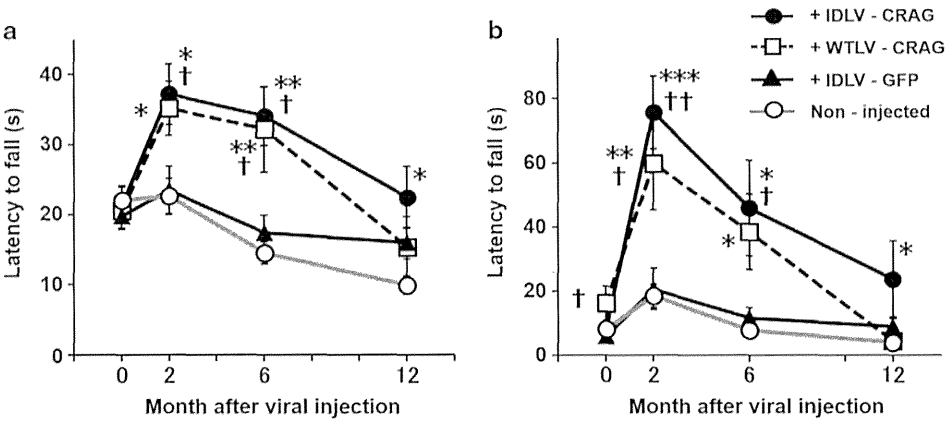

Figure 3. Improvement of the motor behavior of SCA3 mice by cerebellar injection of IDLVs expressing CRAG up to 12 months after the injection. (**a** and **b**) The motor coordination of the mice was tested with a rotating rod. Mice underwent eight trials per day on the accelerating (0–40 r.p.m.) (**a**) rotarod and subsequently the constant (5 r.p.m.) (**b**) rotarod (four trials each) immediately before and at 2, 6 and 12 months after the viral injection. The rotarod performances of non-injected SCA3 mice (non-injected, $n=7$ mice) were compared with those of SCA3 mice injected with WTLVs expressing GFP-P2A-CRAG (+WTLV-CRAG, $n=5$), IDLVs expressing GFP-P2A-CRAG (+IDLV-CRAG, $n=5$) or IDLVs expressing GFP alone (+IDLV-GFP, $n=5$). SCA3 mice injected with IDLVs expressing GFP-P2A-CRAG, but not those injected with IDLVs expressing GFP alone, significantly improved their rotarod performances up to 12 months after the injection compared with the non-injected SCA3 mice. SCA3 mice treated with WTLVs expressing GFP-P2A-CRAG also improved their performance at 2 and 6 months, but not at 12 months, after the injection. $^{*}P<0.05$, $^{**}P<0.01$, $^{***}P<0.001$ (vs non-injected SCA3 mice), $^{\dagger}P<0.05$ and $^{\dagger\dagger}P<0.01$ (vs SCA3 mice expressing GFP alone) by one-way analysis of variance (ANOVA) followed by Tukey's *post hoc* test.

mice. The performance became worse at 12 months after the injection, but still remained significantly better ($P<0.05$) than that of the non-injected control SCA3 mice. SCA3 mice that expressed GFP-P2A-CRAG from WTLVs showed a similar time course as those expressing GFP-P2A-CRAG from IDLVs. However, their performance was indistinguishable from that of non-injected SCA3 mice at 12 months after the injection. Similarly, in the constant speed protocol (Figure 3b), the injection of IDLVs expressing GFP-P2A-CRAG, but not GFP alone, significantly improved rotarod performance at 2 ($P<0.001$), 6 ($P<0.01$) and 12 ($P<0.05$) months after the viral injection compared with non-injected SCA3 mice. SCA3 mice expressing GFP-P2A-CRAG by WTLVs also showed better performance than non-injected SCA3 mice at 2 ($P<0.01$) and 6 ($P<0.05$) months after the injection; however, similar to the accelerating paradigm, their performance was indistinguishable from that of non-injected SCA3 mice at 12 months after the injection.

Significant decrease of the mutant ataxin-3 aggregates by IDLVs expressing CRAG

Viral vector-injected SCA3 mice and non-injected transgenic littermates were killed to examine the effect of CRAG expression on ataxin-3 aggregates in PCs. We examined only the GFP-positive area because GFP-negative areas that had once expressed CRAG from IDLVs and regressed the expression thereafter were indistinguishable from non-infected areas. Thus, although the expression levels of GFP-P2A-CRAG appear similar between WTLV- (Figure 4b) and IDLV-treated (Figure 4c) groups, the GFP-expressing areas were indeed significantly limited in the IDLV-treated cerebella as presented in Figure 2i. Immunohistochemistry for HA tagged with mutant ataxin-3 and calbindin showed numerous large aggregates along the disrupted PC layer in non-injected SCA3 mice (Figures 4a, d, g and j), whereas the number and the size of the aggregates along the PC layer decreased in SCA3 mice expressing CRAG from WTLVs (Figures 4b, e, h and k) or IDLVs (Figures 4c, f, I and l).

We counted the number of PCs along more than 100 μm length of the PC layer from non-injected SCA3 mice and mice expressing CRAG by WTLVs or IDLVs (more than three mice in each group). The average number of PCs per 100 μm length of the PC layer, which was visualized by immunolabeling for calbindin, was not significantly different between non-injected SCA3 mice (6.3 ± 0.5 PCs) and mice treated with WTLVs (7.8 ± 1.1 PCs) or IDLVs (7.8 ± 0.7 PCs) expressing CRAG (Figure 4m). We confirmed that the density of transduced PCs in the regions examined was approximately the same between WTLV- and IDLV-treated SCA3 mice (Figure 4n). Then, we counted the number of aggregates with a diameter over 10 μm^2 along more than 100 μm length of the transduced PC layer. The average number of aggregates in a 100 μm length of the PC layer was significantly decreased by the expression of CRAG by IDLVs (3.9 ± 0.6 aggregates, $P<0.001$), as well as by WTLVs (6.6 ± 0.7 aggregates, $P<0.001$), compared with non-injected control SCA3 mice (15.9 ± 1.9 aggregates) (Figure 4o).

DISCUSSION

In this study, we examined the time course of transgene expression by IDLVs in mouse PCs *in vivo* and assessed the usability of IDLVs for the treatment of SCAs compared with WTLVs using SCA model mice. Two months after the injection of IDLVs expressing GFP, the fluorescence intensity and expression levels of the mRNA in the PC somata were approximately the same as those after the WTLV injection. However, both GFP fluorescence and mRNA levels in IDLV-treated cerebella were significantly decreased at 6 and 12 months after the viral injection. The levels of GFP mRNA in IDLV-treated cerebella were approximately 25% and 5% of those in WTLV-treated cerebella at 6 and 12 months after the injection, respectively. Cerebellar injection of IDLVs expressing CRAG significantly rescued the rotarod performance of SCA3 mice with a time course almost identical to the injection of WTLVs. The performance of SCA3 mice treated with WTLVs was significantly better up to 6 months after the injection, but it became worse thereafter and was indistinguishable from the non-injected control SCA3 mice at 12 months after the injection. Notably, the better performance of SCA3 mice that expressed CRAG from IDLVs continued even 12 months after the injection.

We showed that IDLVs with a mutant gene encoding the D64V integrase had approximately 100 times less ability to integrate the proviral genome into the chromosome of cerebellar neurons *in vivo* compared with WTLVs. This result suggests that the IDLVs have a much lower chance of insertional mutagenesis, which can

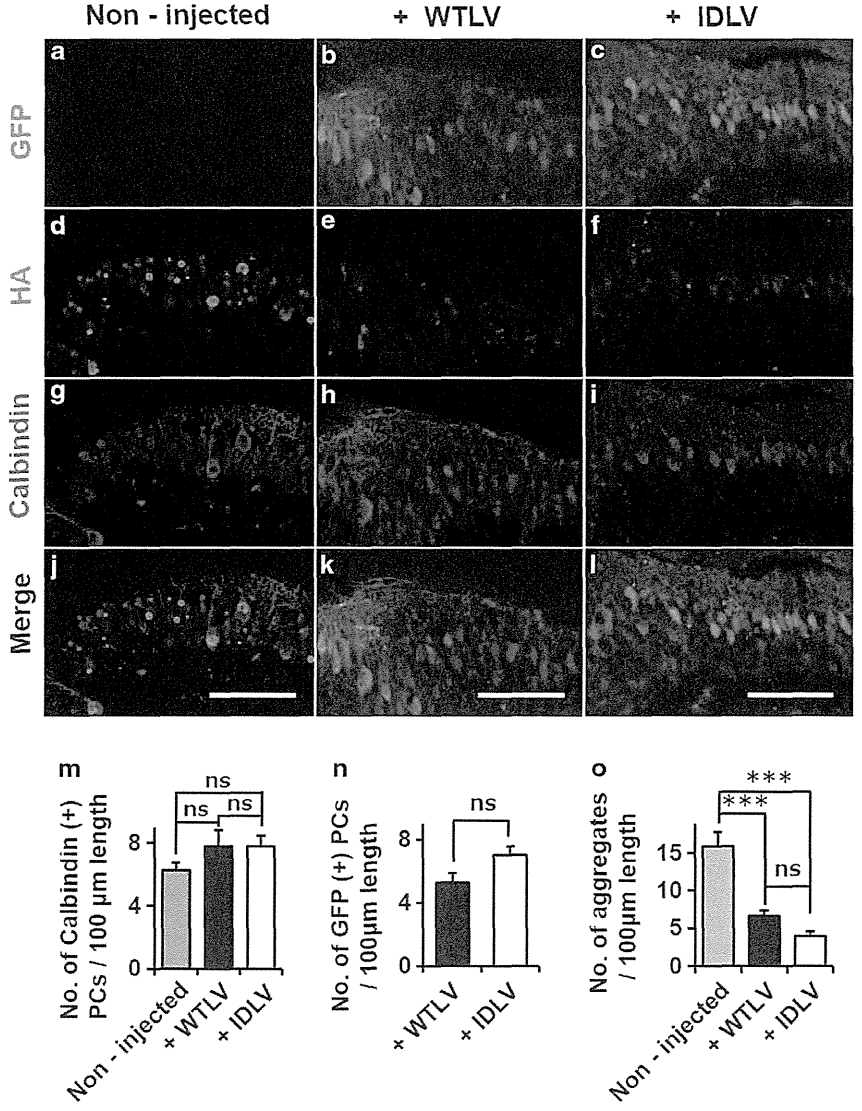

Figure 4. Significant reduction of mutant ataxin-3 aggregates in SCA3 mouse PCs by IDLV-mediated expression of CRAG. (**a**–**l**) Cerebellar slices from SCA3 mice injected with WTLVs (middle panels) or IDLVs (right panels) expressing GFP-P2A-CRAG and those from non-injected SCA3 mice (left panels) were produced at 12 months after the viral injection. The slices were triple immunostained for GFP (**a**–**c**), and HA-tagged mutant ataxin-3 (**d**–**f**) and calbindin (**g**–**i**). The merged images were presented in the lowest panels (**j**–**l**). (**m**) Number of PCs per 100 μm length of the PC layer in slices from non-injected SCA3 mice and mice injected with WTLVs or IDLVs expressing GFP-P2A-CRAG. (**n**) Number of GFP-positive PCs per 100 μm length of the PC layer in slices from non-injected SCA3 mice and mice injected with WTLVs or IDLVs expressing GFP-P2A-CRAG. (**o**) Number of mutant ataxin-3 aggregates per 100 μm length of the PC layer in slices from non-injected SCA3 mice and mice injected with WTLVs or IDLVs expressing GFP-P2A-CRAG. ***$P < 0.001$ by Tukey's *post hoc* test after one-way analysis of variance (ANOVA). NS, not significant. Scale bar, 100 μm.

cause substantial adverse effects. Although the ratio of integration by IDLVs relative to WTLVs was 1/100, IDLVs caused a robust transgene expression in PCs. The expression levels of a transgene were approximately the same as WTLVs at 2 months after injection and declined thereafter.

A previous study showed more efficient human immunodeficiency virus integration in stimulated T cells than in quiescent T cells because of the slower viral life cycle in quiescent cells: human immunodeficiency virus integration peaks 24 h after infection in stimulated cells, whereas it begins 36 h after infection in quiescent cells.[18] The long-terminal repeat ends of the reverse-transcribed viral DNA in the resting cells have higher chances of degradation or processing by cytoplasmic enzymes and the degraded viral DNAs are less efficiently integrated into the host chromosome.[18] Similarly, it is reasonably considered that the integrase-mediated insertion by WTLVs occurs more efficiently in actively dividing HeLa cells than in quiescent neurons *in vivo*, whereas the integrase-independent insertion by cellular recombination enzymes occurs at a similar frequency in HeLa cells and in neurons. In contrast, IDLVs lack the integrase-dependent integration and only show the residual integrase-independent insertion to a similar degree with WTLVs.[11,19] Thus, higher integrase-mediated insertion by WTLVs in HeLa cells than in neurons and a similar frequency of the integrase-independent insertion by WTLVs with that by IDLVs in HeLa cells and neurons could explain the substantial difference in the integration efficiency of IDLVs relative to WTLVs between HeLa cells (1/3850) and neurons *in vivo* (1/111) (Figures 1e and f).

Injection of WTLVs expressing CRAG into the SCA3 mouse cerebella significantly improved their rotarod performance, but

the improved condition did not last long, and the performance returned to a level approximately the same as that of non-injected SCA3 mice. In contrast, IDLV-treated SCA3 mice showed a significantly better performance even at 12 months after the injection. We did not expect these results, as robust transgene expression continued more than 1 year in WTLV-infected cells *in vivo*, whereas the expression in IDLV-infected cells significantly regressed (Figure 2). Overall, the decline of the rotarod performance after 6 months may be explained by the extensive degeneration of PCs in non-transduced lobules, eventually leading to the deterioration of cerebellar function. The reason that explains the inferiority of WTLVs to IDLVs in rotarod performance is not clear, but one possibility is that the continuous overexpression of CRAG and GFP in the WTLV-infected PCs potentiated the endoplasmic reticulum (ER) stress, as the SCA3 mouse PCs are susceptible to the ER stress because of high levels of mutant ataxin-3 expression in PCs. In IDLV-infected PCs, the toxic aggregates were removed by transiently expressed CRAG. Once toxic aggregates are removed in SCA patients, it takes an extended period of time, possibly many years, for the reaccumulation; thus, transient CRAG expression by IDLVs may produce a better therapeutic outcome than continuous CRAG expression, which could enhance the ER stress of affected neurons.

Another problem of using lentiviral vectors for gene therapy is the difficulty in controlling the expression levels of a therapeutic gene. To gain a better and sufficient therapeutic efficacy, the expression levels should fall within a therapeutic window. However, the overexpression of a therapeutic protein could affect cellular function by excessive amounts of the protein itself and/or occupying the cellular protein synthesis machinery by the production of the therapeutic protein (and eventually the suppression of endogenous protein production).[20] Even if such adverse effects are observed, there is currently no way to remove integrated proviruses from host chromosomes. Accommodation of the doxycycline-inducible system in the lentiviral main plasmid may be effective for controlling a transgene expression;[21–23] however, the long-term use of antibiotics, such as doxycycline, also causes significant unwanted effects in patients.[24]

Recently, adeno-associated virus (AAV) vectors have been widely used as gene therapy vectors because of their non-pathogenicity and efficient gene transfer potential.[25–27] However, similar to lentiviral vectors, high levels of transgene expression by AAV vectors also continue for more than several years at minimum.[28,29] In contrast, transgene expression by adenoviral vectors lasts only for a few months in the brain.[30] Although the declining speed of transgene expression by adenoviral vectors may be faster than that by IDLVs, adenoviral vectors have far greater tropism for glial cells than for neurons and exhibit very low transduction efficacy in neurons,[30–32] which may become a problem when gene delivery is targeted to neurons. Moreover, adenoviral vectors have significant immunogenicity,[27,33] which could cause significant damage in infected cells. Thus, IDLVs are thought to be safe from the point of minimum immunogenicity and spontaneous reduction of transgene expression, the latter of which is supposed to initiate several months after viral infection in the brain.

Neurodegenerative diseases, including the major types of SCAs, are caused by the abnormal accumulation of toxic proteins.[34–36] The onset of these diseases occurs, in many cases, during the third or fourth decade of life[34,36] because the disease-causing proteins are degraded through the ubiquitin-proteasome pathway and autophagy in younger individuals.[37–39] As individuals become older, the capacity of degrading unnecessary proteins in neurons is exacerbated, leading to a gradual accumulation of the abnormal proteins. Thus, it requires a long period before disease-causing proteins sufficiently accumulate in neurons to impair neuronal functions and for symptoms to emerge. Here, using SCA3 model mice, we showed that a therapeutic protein, CRAG, could be efficiently expressed in cerebellar neurons *in vivo* by IDLVs, which facilitated the degradation of toxic protein aggregates in PCs. Although the IDLV-mediated expression of the therapeutic protein almost disappears within 1-year after injection, it is thought that it takes an extended period before the disease-causing proteins accumulate again to produce a re-emergence of symptoms in patients. Therefore, IDLVs may essentially be as effective as WTLVs and safer than WTLVs in treating neurodegenerative diseases. Further studies using large animals, such as non-human primates, will warrant the future clinical application of IDLVs.

MATERIALS AND METHODS

Animals

Wild-type C57BL/6 mice were purchased from Japan SLC (Shizuoka, Japan). SCA3 model mice that expressed truncated ataxin-3 with a 69 polyglutamine stretch in PCs were previously generated in our laboratory.[16] Heterozygous SCA3 mice were maintained on a C57BL/6J genetic background by intercrossing fertile wild-type mice in our breeding colony at the Institute of Experimental Animal Research, Gunma University Graduate School of Medicine (Maebashi, Gunma, Japan). Both sexes were used in the experiments. All procedures for the care and treatment of animals were performed according to the Japanese Act on the Welfare and Management of Animals and the Guidelines for Proper Conduct of Animal Experiments issued by the Science Council of Japan. The experimental protocol was approved through the Institutional Committee of Gunma University (No. 09-062). All efforts were made to minimize suffering and reduce the number of animals used.

Plasmids and virus preparation

Human immunodeficiency virus-derived lentiviral vectors, which were pseudotyped with the VSV-G, were used in this study. The lentiviral vector plasmid DNAs were kindly provided by Dr Nienhuis (St Jude Children's Research Hospital, Memphis, TN, USA). The backbones of helper plasmids were derived from pCAGGS.[40] The vectors were designed to express GFP or GFP-P2A-3 × Flag-tagged CRAG under the control of the MSCV promoter. The lentiviral vectors were produced as described previously.[41] Briefly, four plasmids consisting of pCL20c, pCAGkGP1R, pCAG4RTR2 and pCAGVSV-G were co-transfected into HEK293T cells (Thermo Fisher Scientific, Kanagawa, Japan) using the calcium phosphate method. After 48 h, the supernatant containing viral particles was harvested and ultracentrifuged (CP80WX; Hitachi Koki, Tokyo, Japan). The precipitated viral particles were resuspended in 70 μl of Dulbecco's phosphate-buffered saline (−). The genome titers of WTLVs and IDLVs were determined using a known titer samples as a standard, except for lentiviral vectors expressing GFP-P2A-3 × Flag-tagged CRAG. To confirm that the titers of WTLVs expressing GFP-P2A-3 × Flag-tagged CRAG were therapeutically effective, that is, the titers were equal or higher than those used in our previous experiments,[16] the biologic titers (transduction units ml^{-1}) were determined by counting the number of GFP-expressing cells after transducing HEK293T cells, as described.[41] The lentiviral solution was stored at 4 °C and used within 2 weeks.

Western blot analysis

Viral solutions were solubilized with lysis buffer containing 50 mM phosphate buffer (pH 7.4) and 2% (w v^{-1}) sodium dodecyl sulfate. Solubilized solutions were added with the same volume of sample buffer, which contained 125 mM Tris-HCl (pH 6.8), 4% (w v^{-1}) sodium dodecyl sulfate, 10% (v v^{-1}) mercapto-EtOH, 20% (v v^{-1}) glycerol and 0.001% (w v^{-1}) bromophenol blue and were incubated for 25 min at 55 °C. Samples were electrophoresed on sodium dodecyl sulfate-polyacrylamide gels (5–15%) and transferred to nitrocellulose membranes (BioTrace NT Nitrocellulose Transfer Membrane; PALL Co., Port Washington, NY, USA). The membranes were blocked with 5% non-fat skimmed milk in phosphate-buffered saline containing 0.05% Tween-20. The immunoreaction was performed with rabbit polyclonal anti-VSV-G antibodies (1:4000; Sigma), followed by the incubation of horseradish peroxidase-conjugated anti-rabbit IgG (Bio-Rad, Tokyo, Japan) at a 1:40 000 dilution. Immunoreactive bands were visualized using an enhanced chemiluminescence reagent (Clarity Western ECL Substrate; Bio-Rad). The relative amount of immunoreactive VSV-G band in each lane was quantified with ImageJ software (http://rsb.info.nih.gov/ij/).

Viral injection into mouse cerebellum

Mice were anesthetized before and throughout the viral injection using 2% isoflurane inhalation (flow speed: 1 l min^{-1}) with the mouse mounted on a stereotactic frame. A burr hole was drilled on the surface of the cerebellar vermis, which was located 5–6 mm caudal to the bregma. The blunt-ended tip (33 G) of a Hamilton syringe attached to a micropump (UltramicroPump II; World Precision Instruments (WPI), Sarasota, FL, USA) was placed immediately below the pia mater of the cerebellar vermis. Ten microliters of viral solution was injected at a rate of 300 nl min^{-1}. The temporal change of a transgene expression after IDLV or WTLV infection in mouse cerebellum *in vivo* (Figure 2) was examined using 29 mice. The therapeutic effect of CRAG expression by IDLVs or WTLVs (Figure 3) was explored using 34 mice.

Quantitative Alu-PCR

To purify the chromosomal DNA from HeLa cells, the cells were seeded on a 6-cm culture dish at a density of 1×10^5 cells in the medium, which contained 1 µl of WTLVs or the same volume of genomic titer-adjusted IDLVs and Polybrene (final concentration: 6 µg ml^{-1}). Four days after cultivation, HeLa cells were collected using a plastic scraper after washing with ice-cold PBS. HeLa cells without viral infection were used as negative controls. Chromosomal DNA was purified using a Genomic DNA Purification System (A2361; Promega, Madison, WI, USA). The integrated transgene was detected by nested Alu-PCR. The details of the Alu-PCR protocol have been described in a previous report.[42] The first PCR was carried out using a forward primer that was targeted to the long-terminal repeat from the retroviral sequence (LM-667, 5′-ATGCCACGTAAGCGAAACT CTGGCTAACTAGGGAACCCACTG-3′), which was attached to a lambda phage-specific heel sequence at the 5′ side; this method was used to avoid amplification of the non-integrated transgene derived from the lentiviral vector, as well as one-long-terminal repeat or two-long-terminal repeat circular DNA. Reverse primers were targeted to the Alu sequences present in the host genomic DNA (Alu1, 5′-TCCCAGCTACTGGGGAGGCTGAGG-3′; Alu2, 5′-GCCTCCCAAAGTGCTGGGATTACA-3′). The first reaction was performed using PrimeStar Max (Takara Bio, Shiga, Japan) with three primers, including LM-667, Alu1 and Alu2, in 20 µl of reaction volume. The thermal cycler was programmed to perform a hot start at 98 °C for 10 s, 60 °C for 5 s and 72 °C for 2 min. The second real-time quantitative PCR was performed using 2 µl of the first PCR product. The reactions were performed using SYBER Premix EX Taq II (Takara Bio) with the addition of two nested primers (LambdaT, 5′-ATGCCACGTAAGCGAAAC T-3′, and AA55M, 5′-GCTAGAGATTTTCCACACTGACTAA-3′) in 25 µl of reaction volume. The real-time PCR was conducted using a Thermal Cycler Dice TP800 (Takara Bio) with a hot start at 95 °C for 10 s, followed by 40 cycles of 95 °C for 5 s and 60 °C for 30 s. The following glyceraldehyde 3-phosphate dehydrogenase primers were used for normalization in the second PCR: forward, 5′-TGTGTCCGTCGTGGATCTGA-3′ and reverse, 5′-TTGCTGTTGAAG TCGCAGCAG-3′.

Quantitative B1-PCR

To investigate the efficiency of the proviral integration into the mouse brain, we used a mouse B1 sequence,[43] instead of a human Alu sequence.[44] The mouse B1 sequence is a homologous repeat sequence of the human Alu sequence, and these sequences belong to short interspersed elements.[45] Ten microliters of WTLVs or the same volume of IDLVs were injected into the cerebellar vermis of P27–28 mice ($n = 5$ mice, respectively). One week after the injection, the GFP-expressing cerebellar vermis was excised from the whole cerebellum under a fluorescence microscope. Then, the tissue was homogenized immediately in the lysis buffer containing proteinase K. After overnight incubation at 60 °C, genomic DNAs were harvested using the phenol–chloroform and ethanol precipitation method. The genomic samples were finally diluted to 10–15 ng $µl^{-1}$ with TE buffer and used for PCR analysis. The procedure for the nested B1-PCR was essentially the same as for the nested Alu-PCR. The first PCR was performed using KOD FX Neo (Toyobo, Osaka, Japan) and three different primers. One primer was a lambda phage sequence-tagged GFP forward primer (5′-ATGCCACGTAAGCGAAACTCGACCACTACCAGCAG AACAC-3′), whereas the others were sense and antisense primers targeted to the B1 sequence (sense, 5′-TCTACAAAGTGAGTTCCAGGACAGCCAGGG-3′ and antisense, 5′-CCCTGGCTGTCCTGGAACTCACTTTGTAG-3′). The thermal cycler was programmed to perform 20 cycles of 98 °C for 10 s, 60 °C for 30 s and 68 °C for 5 min. The first PCR products were diluted 100-fold and used as a template for the second real-time PCR. The second real-time PCR was performed using a KAPA SYBR FAST qPCR Kit (Nippon Genetics, Tokyo, Japan) and paired primers targeted to the lambda phase tag (5′-ATGCCACGTAAGCGAAACT-3′) and the GFP sequence (5′-TGTGATCG CGCTTCTCGTTGG-3′). The real-time PCR was performed at 45 cycles of 95 °C for 3 s and 60 °C for 30 s. Glyceraldehyde 3-phosphate dehydrogenase was used to normalize the variation derived from the difference in each sample volume.

Quantitative reverse transcriptase-PCR

The amount of genomic RNA in lentiviral particles and that of mRNA of GFP expressed in mouse cerebellum were examined by quantitative reverse transcriptase-PCR. Total RNA was extracted using a RNA isolation kit (RNeasy Mini kit; Qiagen, Hilden, Germany) and reverse transcribed with the ReverTra Ace qPCR RT kit (Toyobo). The quantitative reverse transcriptase-PCR was performed using a THUNDERBIRD SYBR qPCR Mix (Toyobo) with the addition of the following primer sets: amplification of the viral genome containing the MSCV promoter, MSCV-F, 5′-CACTCCCTTA AGTTTGACCTT-3′ and MSCV-R, 5′-GCCAAGGCTTCCCAGGTC-3′, and the amplification of the GFP gene from mouse cerebellum, GFP-F, 5′-CGACCAC TACCAGCAGAACAC-3′ and GFP-R, 5′-TGTGATCGCGCTTCTCGTTGG-3′. The PCR was performed for 40 cycles consisting of 95 °C for 5 s followed by 60 °C for 30 s. Glyceraldehyde 3-phosphate dehydrogenase was used to normalize the variation derived from the difference in each sample volume.

Rotarod test

The motor control ability of SCA3 mice was assessed by a rotarod (Muromachi Kikai, Tokyo, Japan) with two different paradigms. In the accelerated paradigm, the rod accelerated from 0 to 40 r.p.m. in 3 min, whereas in the stable speed paradigm, the rod rotated at a stable speed of 5 r.p.m. Mice were assessed with both paradigms immediately before and 2, 6 and 12 months after the viral injection. In the accelerating and stably rotating tests, mice were subjected to four and six trials, respectively, with a 30 min rest between the trials. The average latency to fall from the rod was examined. Seven non-injected control mice and five lentivirally treated mice from each group were examined.

Immunohistochemistry

Mice were transcardially perfused with 4% paraformaldehyde in 0.1 M phosphate buffer after they were anesthetized with a combination of ketamine (100 mg kg^{-1} body weight) and xylazine (10 mg kg^{-1} body weight). The brains were then postfixed in the same fixative for 24 h. For immunostaining, the cerebellum was cut into 50 µm sagittal sections using a microslicer (VT1000S; Leica, Nussloch, Germany). Floating sections were immunostained with rabbit polyclonal anti-GFP antibody (1:500; Frontier institute, Hokkaido, Japan), rat monoclonal anti-HA (1:500; Roche, Basel, Switzerland) and mouse monoclonal anti-calbindin D-28K (1:500; Swant, Bellinzona, Switzerland) and visualized with Alexa Fluor 488-conjugated anti-rabbit IgG, Alexa Fluor 568-conjugated anti-rat IgG and Alexa Fluor 680-conjugated anti-mouse IgG (1:1000; Life Technologies, Carlsbad, CA, USA).

Confocal microscopy

Photographs of the whole brain were obtained by fluorescent stereoscopic microscopy (VBG25; Keyence, Osaka, Japan). The brains from lentivirally treated or non-treated mice ($n = 3$ mice from each group) were then postfixed in the same fixative for 24 h. The cerebellum was cut into 50-µm sagittal sections using a microslicer (VT1000S; Leica). Immunohistochemical images were obtained by a confocal laser-scanning microscope (LSM 5 PASCAL; Zeiss, Oberkochen, Germany). Serial confocal scanning images were obtained using optical sectioning with 1 µm slices and were reconstructed three dimensionally. Sizes of ataxin-3 aggregates in PCs were assessed with Image Analysis Software (WinROOF; Mitani Corporation, Fukui, Japan).

Measurement of GFP fluorescence intensity in PC somata

Native GFP fluorescence images of the cerebellar cortex (Figure 2) were taken with a confocal microscope. For comparison of GFP fluorescence intensity between different animals, the images were always obtained with the same condition. In each experimental group, more than 100 PCs from three mice were measured with Image Analysis Software (WinROOF).

Statistical analysis

Significant differences were analyzed by Tukey's *post hoc* test after one-way analysis of variance using the R software statistical package (http://www.r-project.org) or an unpaired *t*-test. Data are expressed as the mean ± s.e.m.

CONFLICT OF INTEREST

The authors declare no conflict of interest.

ACKNOWLEDGEMENTS

We thank Junko Sugiyama, Asako Onishi and Hiromi Hirai for maintaining and genotyping the mutant mice. This work was supported by a grant from the Funding Program for Next Generation World-Leading Researchers (LS021) (to HH) and a Grant-in-Aid from the Japan Society for the Promotion of Science (JSPS); Grant-in-Aid for Young Scientists (B) KAKENHI 22700374).

REFERENCES

1 Lever AM, Strappe PM, Zhao J. Lentiviral vectors. *J Biomed Sci* 2004; **11**: 439–449.
2 Apolonia L, Waddington SN, Fernandes C, Ward NJ, Bouma G, Blundell MP *et al.* Stable gene transfer to muscle using non-integrating lentiviral vectors. *Mol Ther* 2007; **15**: 1947–1954.
3 Kulkosky J, Skalka AM. Molecular mechanism of retroviral DNA integration. *Pharmacol Ther* 1994; **61**: 185–203.
4 Hindmarsh P, Leis J. Retroviral DNA integration. *Microbiol Mol Biol Rev* 1999; **63**: 836–843; table of contents.
5 Hacein-Bey-Abina S, Von Kalle C, Schmidt M, McCormack MP, Wulffraat N, Leboulch P *et al.* LMO2-associated clonal T cell proliferation in two patients after gene therapy for SCID-X1. *Science* 2003; **302**: 415–419.
6 Li Z, Dullmann J, Schiedlmeier B, Schmidt M, von Kalle C, Meyer J *et al.* Murine leukemia induced by retroviral gene marking. *Science* 2002; **296**: 497.
7 Matrai J, Chuah MK, VandenDriessche T. Recent advances in lentiviral vector development and applications. *Mol Ther* 2010; **18**: 477–490.
8 Banasik MB, McCray Jr PB. Integrase-defective lentiviral vectors: progress and applications. *Gene Therapy* 2010; **17**: 150–157.
9 Bayer M, Kantor B, Cockrell A, Ma H, Zeithaml B, Li X *et al.* A large U3 deletion causes increased *in vivo* expression from a nonintegrating lentiviral vector. *Mol Ther* 2008; **16**: 1968–1976.
10 Lombardo A, Genovese P, Beausejour CM, Colleoni S, Lee YL, Kim KA *et al.* Gene editing in human stem cells using zinc finger nucleases and integrase-defective lentiviral vector delivery. *Nat Biotechnol* 2007; **25**: 1298–1306.
11 Nightingale SJ, Hollis RP, Pepper KA, Petersen D, Yu XJ, Yang C *et al.* Transient gene expression by nonintegrating lentiviral vectors. *Mol Ther* 2006; **13**: 1121–1132.
12 Philippe S, Sarkis C, Barkats M, Mammeri H, Ladroue C, Petit C *et al.* Lentiviral vectors with a defective integrase allow efficient and sustained transgene expression *in vitro* and *in vivo*. *Proc Natl Acad Sci USA* 2006; **103**: 17684–17689.
13 Saenz DT, Loewen N, Peretz M, Whitwam T, Barraza R, Howell KG *et al.* Unintegrated lentivirus DNA persistence and accessibility to expression in non-dividing cells: analysis with class I integrase mutants. *J Virol* 2004; **78**: 2906–2920.
14 Yanez-Munoz RJ, Balaggan KS, MacNeil A, Howe SJ, Schmidt M, Smith AJ *et al.* Effective gene therapy with nonintegrating lentiviral vectors. *Nat Med* 2006; **12**: 348–353.
15 Qin Q, Inatome R, Hotta A, Kojima M, Yamamura H, Hirai H *et al.* A novel GTPase, CRAG, mediates promyelocytic leukemia protein-associated nuclear body formation and degradation of expanded polyglutamine protein. *J Cell Biol* 2006; **172**: 497–504.
16 Torashima T, Koyama C, Iizuka A, Mitsumura K, Takayama K, Yanagi S *et al.* Lentivector-mediated rescue from cerebellar ataxia in a mouse model of spinocerebellar ataxia. *EMBO Rep* 2008; **9**: 393–399.
17 Leavitt AD, Robles G, Alesandro N, Varmus HE. Human immunodeficiency virus type 1 integrase mutants retain *in vitro* integrase activity yet fail to integrate viral DNA efficiently during infection. *J Virol* 1996; **70**: 721–728.
18 Vatakis DN, Kim S, Kim N, Chow SA, Zack JA. Human immunodeficiency virus integration efficiency and site selection in quiescent CD4+ T cells. *J Virol* 2009; **83**: 6222–6233.
19 Nakajima N, Lu R, Engelman A. Human immunodeficiency virus type 1 replication in the absence of integrase-mediated dna recombination: definition of permissive and nonpermissive T-cell lines. *J Virol* 2001; **75**: 7944–7955.
20 Sawada Y, Kajiwara G, Iizuka A, Takayama K, Shuvaev AN, Koyama C *et al.* High transgene expression by lentiviral vectors causes maldevelopment of Purkinje cells *in vivo*. *Cerebellum* 2010; **9**: 291–302.
21 Liu B, Wang S, Brenner M, Paton JF, Kasparov S. Enhancement of cell-specific transgene expression from a Tet-Off regulatory system using a transcriptional amplification strategy in the rat brain. *J Gene Med* 2008; **10**: 583–592.
22 Hioki H, Kuramoto E, Konno M, Kameda H, Takahashi Y, Nakano T *et al.* High-level transgene expression in neurons by lentivirus with Tet-Off system. *Neurosci Res* 2009; **63**: 149–154.
23 Kobayashi K, Yasuhara T, Agari T, Muraoka K, Kameda M, Ji Yuan W *et al.* Control of dopamine-secretion by Tet-Off system in an *in vivo* model of parkinsonian rat. *Brain Res* 2006; **1102**: 1–11.
24 Sloan B, Scheinfeld N. The use and safety of doxycycline hyclate and other second-generation tetracyclines. *Expert Opin Drug Saf* 2008; **7**: 571–577.
25 Vandenberghe LH, Auricchio A. Novel adeno-associated viral vectors for retinal gene therapy. *Gene Therapy* 2012; **19**: 162–168.
26 Weinberg MS, Samulski RJ, McCown TJ. Adeno-associated virus (AAV) gene therapy for neurological disease. *Neuropharmacology* 2013; **69**: 82–88.
27 Lentz TB, Gray SJ, Samulski RJ. Viral vectors for gene delivery to the central nervous system. *Neurobiol Dis* 2012; **48**: 179–188.
28 Stieger K, Schroeder J, Provost N, Mendes-Madeira A, Belbellaa B, Le Meur G *et al.* Detection of intact rAAV particles up to 6 years after successful gene transfer in the retina of dogs and primates. *Mol Ther 2009*; **17**: 516–523.
29 Niemeyer GP, Herzog RW, Mount J, Arruda VR, Tillson DM, Hathcock J *et al.* Long-term correction of inhibitor-prone hemophilia B dogs treated with liver-directed AAV2-mediated factor IX gene therapy. *Blood* 2009; **113**: 797–806.
30 Terashima T, Miwa A, Kanegae Y, Saito I, Okado H. Retrograde and anterograde labeling of cerebellar afferent projection by the injection of recombinant adenoviral vectors into the mouse cerebellar cortex. *Anat Embryol* 1997; **196**: 363–382.
31 Iino M, Goto K, Kakegawa W, Okado H, Sudo M, Ishiuchi S *et al.* Glia-synapse interaction through Ca^{2+}-permeable AMPA receptors in Bergmann glia. *Science* 2001; **292**: 926–929.
32 Duale H, Kasparov S, Paton JF, Teschemacher AG. Differences in transductional tropism of adenoviral and lentiviral vectors in the rat brainstem. *Exp Physiol* 2005; **90**: 71–78.
33 Hartman ZC, Appledorn DM, Amalfitano A. Adenovirus vector induced innate immune responses: impact upon efficacy and toxicity in gene therapy and vaccine applications. *Virus Res* 2008; **132**: 1–14.
34 Johnson WG. Late-onset neurodegenerative diseases—the role of protein insolubility. *J Anat* 2000; **196** (Part 4): 609–616.
35 Nagai Y, Popiel HA. Conformational changes and aggregation of expanded polyglutamine proteins as therapeutic targets of the polyglutamine diseases: exposed beta-sheet hypothesis. *Curr Pharm Des* 2008; **14**: 3267–3279.
36 Seidel K, Siswanto S, Brunt ER, den Dunnen W, Korf HW, Rub U. Brain pathology of spinocerebellar ataxias. *Acta Neuropathol* 2012; **124**: 1–21.
37 Williams A, Jahreiss L, Sarkar S, Saiki S, Menzies FM, Ravikumar B *et al.* Aggregate-prone proteins are cleared from the cytosol by autophagy: therapeutic implications. *Curr Top Dev Biol* 2006; **76**: 89–101.
38 Hegde AN, Upadhya SC. Role of ubiquitin-proteasome-mediated proteolysis in nervous system disease. *Biochim Biophys Acta* 2011; **1809**: 128–140.
39 Takalo M, Salminen A, Soininen H, Hiltunen M, Haapasalo A. Protein aggregation and degradation mechanisms in neurodegenerative diseases. *Am J Neurodegen Dis* 2013; **2**: 1–14.
40 Niwa H, Yamamura K, Miyazaki J. Efficient selection for high-expression transfectants with a novel eukaryotic vector. *Gene* 1991; **108**: 193–199.
41 Torashima T, Yamada N, Itoh M, Yamamoto A, Hirai H. Exposure of lentiviral vectors to subneutral pH shifts the tropism from Purkinje cell to Bergmann glia. *Eur J Neurosci* 2006; **24**: 371–380.
42 Brussel A, Delelis O, Sonigo P. Alu-LTR real-time nested PCR assay for quantifying integrated HIV-1 DNA. *Methods Mol Biol* 2005; **304**: 139–154.
43 Kass DH, Raynor ME, Williams TM. Evolutionary history of B1 retroposons in the genus Mus. *J Mol Evol* 2000; **51**: 256–264.
44 Nelson DL, Ledbetter SA, Corbo L, Victoria MF, Ramirez-Solis R, Webster TD *et al.* Alu polymerase chain reaction: a method for rapid isolation of human-specific sequences from complex DNA sources. *Proc Natl Acad Sci USA* 1989; **86**: 6686–6690.
45 Waterston RH, Lindblad-Toh K, Birney E, Rogers J, Abril JF, Agarwal P *et al.* Initial sequencing and comparative analysis of the mouse genome. *Nature* 2002; **420**: 520–562.

Cerebellum
DOI 10.1007/s12311-014-0604-1

REVIEW

Mesenchymal Stem Cells as a Potential Therapeutic Tool for Spinocerebellar Ataxia

Kazuhiro Nakamura · Tokue Mieda · Nana Suto · Serina Matsuura · Hirokazu Hirai

Abstract Spinocerebellar ataxia (SCA) is a devastating progressive neurodegenerative disorder, for which no effective treatments have been developed. However, some studies have shown that an intracerebellar or intrathecal injection of mesenchymal stem cells (MSCs) was partially effective in some genetic mouse models of cerebellar ataxia such as SCA1 and *Lurcher* mutant. MSCs likely exert their therapeutic efficacy by secreting innate factors to induce neuronal growth and synaptic connection and reduce apoptosis. In this review, we introduce the therapeutic influence of MSCs on each mouse model for cerebellar ataxia and the possible mechanisms underlying the action of MSCs. We also introduce studies on the safety and effectiveness of umbilical cord MSCs for patients with SCA.

Keywords Mesenchymal stem cells · Motor coordination · Mouse · Purkinje cells · Spinocerebellar ataxia

Introduction

The degeneration of neurons in brain regions such as the brainstem, cerebellum, spinocerebellar tracts, and their afferent/efferent connections leads to ataxia (reviewed in [1]). Currently, over 50 different types of inherited ataxias have been reported [2, 3], including spinocerebellar ataxia (SCA), which is a major neurodegenerative disorder. Among various types of the SCA, autosomal dominantly inherited polyglutamine diseases are the most frequent types and are caused by the expansion of a CAG trinucleotide repeat in the coding region of causative genes. For instance, SCA type 1 (SCA1) is caused by ataxin-1 protein (ATXN1) with an abnormally expanded polyglutamine stretch [4] and is characterized by neurodegeneration in a wide range of the central nervous system (CNS) and the peripheral nervous system (PNS) [5] including the cerebral cortex, basal ganglia, brainstem, cerebellum, and spinal cord. The disease begins with cerebellar ataxia and is often associated with other neurological signs such as pyramidal signs, ophthalmoplegia, and cognitive impairment [6]. So far, no effective approach has been presented for reversing the symptoms of SCA1 patients.

Currently, gene therapy and stem cell therapy have been tested using mouse models for SCA to look for effective treatments. Historically, gene therapies for SCA have been extensively developed earlier than stem cell therapy. In a study utilizing gene therapy to treat CNS pathology of SCA1 transgenic (SCA1-Tg) mice that express a transgene containing the ATXN1 sequence with an 82 CAG repeat expansion specifically in cerebellar Purkinje cells (PCs) [7, 8], an intracerebellar injection of recombinant adeno-associated viral vectors expressing short hairpin RNAs targeting ATXN1 messenger RNA (mRNA) significantly reduced the intranuclear inclusions that are characteristic of the SCA1 in PCs, attenuated the disorganization of the cerebellar morphology, and profoundly improved motor coordination in these mice [9]. The above work was based on the idea that the level of the polyglutamine-expanded protein is one of the critical factors that contributes to disease severity. This idea was further confirmed in another study showing that an attenuation of cytotoxicity was mediated by microRNA-mediated decreases in the polyglutamine-expanded ATXN1 [10]. Vesicular stomatitis virus glycoprotein (VSV-G) pseudotyped

K. Nakamura · N. Suto · S. Matsuura · H. Hirai (✉)
Department of Neurophysiology, Gunma University Graduate School of Medicine, 3-39-22 Showa-machi, Maebashi, Gunma 371-8511, Japan
e-mail: hirai@gunma-u.ac.jp

T. Mieda
Orthopedic Surgery, Gunma University Graduate School of Medicine, 3-39-22 Showa-machi, Maebashi, Gunma 371-8511, Japan

Published online: 04 October 2014

lentiviral vectors have also been used to overexpress genes of interest in neurons because the viral vectors have a high tropism for neurons and enable the efficient and continuous expression of foreign genes for at least a couple of years [11]. Furthermore, the viral vectors can infect neuronal cells without significant toxicity [12]. As a successful example of treating SCA model mice using lentiviral vectors, the overexpression of collapsin response mediator protein-associated molecule-associated guanosine triphosphatase (CRAG), a molecule that facilitates the ubiquitin proteasome pathway, in the cerebellum reduced the neuronal pathology and ameliorated the behavioral defect observed in SCA3 mice [13].

Recently, stem cell therapy for SCA mice was also tested. The injection of neural precursor cells (NPCs) derived from the subventricular zone into the cerebellar white matter of SCA1-Tg mice promoted both the recovery of motor behavior and morphological improvement in PCs [14]. Similar to NPCs, mesenchymal stem cells (MSCs) have been studied for their potential clinical use in the treatment of neurodegenerative disorders [15] and stroke [16, 17]. MSCs are defined as multi-potent progenitor cells that can differentiate into mesenchymal lineage cells, such as osteoblasts, adipocytes, and chondrocytes, and into other cell lineages, such as glial cells and hepatocytes [18–20]. MSCs can easily be isolated from multiple sources that include umbilical cord blood, bone marrow, and adipose tissue [21–23]. MSCs are characterized by the expression of the surface markers CD73, CD90, and CD105 and are negative for CD11b, CD14, CD19, CD79a, CD34, CD45, and HLA-DR [24]. For cerebellar ataxia, MSCs have been tested in *Lurcher* mutant mice. The intracerebellar transplantation of bone marrow-derived MSCs into the cerebellum improves the motor function of *Lurcher* mice [25], which are characterized by a spontaneous frameshift mutation in the δ2 glutamate receptor gene [26]. In contrast to the study above, in which MSCs were injected into the brain parenchyma, MSCs were intrathecally administered to SCA1-Tg mice in our latest study [27]. Mouse bone marrow-derived MSCs significantly ameliorated the ectopic expression of PCs, atrophy of PC dendrites, and progressive motor incoordination observed in the SCA1-Tg mice [27]. In the following sections, we discuss possible mechanisms by which MSCs reduced the degeneration of PCs.

Efficacy of MSCs in Treating Mouse Models for Cerebellar Ataxia

Few studies have used MSCs to treat mouse models for cerebellar ataxia. The first attempt was to use pharmacologically induced ataxic animals. Ataxic mice were induced by cytosine beta-D-arabinofuranoside, after which human umbilical MSCs were injected into these mice [28]. The ataxic mice were given an intravenous injection of 2×10^6 human umbilical MSCs once a week for three consecutive weeks. Human umbilical MSCs significantly improved the motor skills of ataxic mice 8 weeks after the application. Human umbilical MSCs also alleviated cerebellar atrophy and decreased the number of apoptotic cells in the treated mice. Thus, human umbilical MSCs effectively reduced both the morphological and behavioral deficits observed in the pharmacologically degenerated mice.

The second approach was to test the efficacy of MSCs using ataxic mice with spontaneous mutation or transgene expression. Bone marrow-derived MSCs were transplanted into the cerebellum of newborn *Lurcher* mice [25], which are characterized by a spontaneous frameshift mutation in the δ2 glutamate receptor gene [26]. Two months after the surgical procedure, the treated mice presented significant improvements in the motor behavior tests performed. Histological analysis of the cerebellum indicated that the donor cells had migrated throughout the cerebellum and indicated a significant preservation of the number of PCs.

The injection of MSCs into the cerebellum of *Lurcher* mice requires a highly invasive operation that damages the multilayered neck muscles and opens a burr hole. Instead, we chose to intrathecally inject SCA1 mice because this route of administration requires a minimally invasive procedure that is readily applicable to patients in an outpatient clinic. We first checked whether the intrathecally injected MSCs actually reached the brain parenchyma. MSCs injected into the meninges should pass through the pia mater and enter the brain tissue. This turned out to be true: MSCs that had been injected into the meninges above the superior colliculus just rostral to the cerebellum in mice were detected in lobules 3, 4, 5, and 6 of the cerebellum and in the spaces between the folia [27].

Because we sought to start treatment during the presymptomatic stage, we intrathecally injected mouse bone marrow-derived MSCs into SCA1-Tg mice at 5 weeks of age, when the ataxia of the transgenic animals is not so severe [7, 8]. As for the number of MSCs injected into the mice, at least 10^5–10^6 cells were used in other studies of MSC transplantation into a mouse model of another type of cerebellar ataxia [25]. However, we applied a single intrathecal injection of just 3×10^3 MSCs into the mice. This dosage (1×10^5 cells/kg body weight of mice) is close to that used in a recent study, in which patients with multiple sclerosis received a single intrathecal injection (29.5×10^6 cells corresponding to approximately 5×10^5 cells/kg body weight) [29].

The cerebella of untreated SCA1-Tg mice had ectopically located PC somata forming multi-PC layer alignment at 21–23 weeks of age. As demonstrated in previous studies that have shown noticeable atrophy of the molecular layer in 15-week-old SCA1-Tg mice [8], the molecular layer in the untreated SCA1-Tg mice was thinner [27]. Upon the intrathecal injection of MSCs, the treated SCA1-Tg mice displayed a single layer of PC soma without ectopically located cell

bodies and a molecular layer that was thicker than that of the untreated SCA1-Tg mice [27]. Similarly, most of the dendrites of the PCs of the untreated SCA1-Tg mice were shorter and less branched. After treatment with MSCs, the SCA1-Tg mice exhibited a significant preservation of dendrites (Fig. 1). More detailed morphological analysis of PC dendrites revealed that the decrease in the spine density was significantly suppressed after the injection (Fig. 1) [27]. Together, intrathecally injected MSCs effectively ameliorated the degeneration of PCs.

The morphological preservation induced by the MSC transplantation resulted in behavioral recovery in treated SCA1-Tg mice. Motor coordination was repeatedly tested by the rotarod test from 5 weeks after the MSC transplant (10 weeks of age). The MSC-treated mice steadily improved their performance to a level that was indistinguishable from that of wild-type mice from 11 to 20 weeks of age in both accelerating and constant speed protocols [27].

A study that injected NPCs derived from the subventricular zone into three sites (1×10^5 cells at each site) of the cerebellar white matter of the same SCA1-Tg mice applied a nearly identical accelerating rotarod protocol (4–40 rpm, four trials per day) [14]. Therefore, the comparison of the NPC-injected results with those of the MSC injection is informative regarding the optimal conditions for stem cell therapy for SCA1. Although the NPC grafting was effective for aged SCA1-Tg mice at approximately 24 weeks of age, when significant PC loss had occurred, this treatment was not effective for the younger SCA1-Tg mice given the NPC transplantation at 5 or 13 weeks. These observations suggest that NPCs specifically migrate toward substantially degenerated PCs (24 weeks old) and exert their therapeutic effects. In contrast, we intrathecally injected MSCs before apparent neurodegeneration and observed an almost complete suppression of progressive motor deficits. Thus, MSCs, but not NPCs, may have the potential to target less-degenerated PCs.

Actions of Administered MSCs on Neurons

Many researchers working on stem cell therapy for neurodegenerative disorders have focused on MSCs because of their safety and easy isolation and expansion (reviewed in [30]). Regarding safety, MSCs do not show adverse events or rejection reactions [31, 32]. In addition, MSCs shield themselves from the immune system [33], which enables transplantation without tissue matching.

Human MSCs are known to secrete a variety of growth factors that have both paracrine and autocrine activities in the

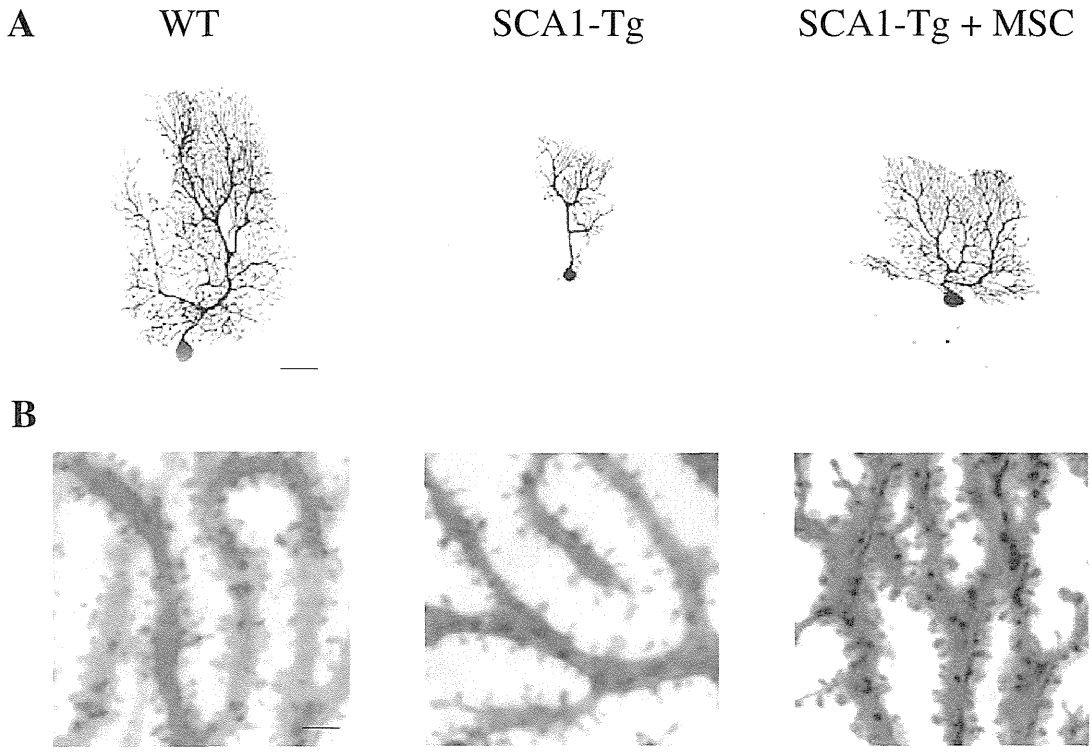

Fig. 1 Intrathecal injection of MSCs ameliorated degeneration of PCs of SCA1-Tg mice. Three thousand MSCs were intrathecally injected to the 5-week-old SCA1-Tg mice, and the PC morphology was examined at 21–23 weeks of age. Representative images of biocytin-injected PC dendrites (**a**) and magnified spines (**b**) from wild-type (WT), naïve SCA1-Tg, and MSC-injected SCA1-Tg mice are shown. Both the total dendritic area of the PCs (**a**) and the number of spines originating from the 10-μm-long dendritic shafts of the biocytin-injected PCs (**b**) were significantly mitigated by intrathecal injection of MSCs. *Scale bars*, 50 μm (**a**) and 2 μm (**b**). The images in **b** were reproduced from our published paper [27]

damaged brain [34]. MSCs target injured areas and release trophic factors that can suppress local inflammation; enhance angiogenesis; reduce free radical levels; inhibit fibrosis and apoptosis; and stimulate the recruitment, retention, proliferation, and differentiation of tissue-residing stem cells [35].

The number of engrafted MSCs was consistently low in the damaged tissue, suggesting that their efficacy relies on actions other than the direct differentiation of MSCs into neurons and/or glia [30]. Instead, trophic factors released from MSCs might act on neurons because hepatocyte growth factor (HGF), fibroblast growth factor-2 (FGF-2), insulin-like growth factor-1 (IGF-1), and vascular endothelial growth factor (VEGF) have all been detected in MSC-conditioned medium [30]. Indeed, human umbilical MSC-treated mice showed higher levels of IGF-1 and VEGF in the cerebellum and peripheral blood circulation in ataxic mice induced by cytosine beta-D-arabinofuranoside [28]. The extracellular matrix molecules produced by MSCs have also been shown to support neural cell attachment, growth, and axonal extension [36].

How are MSC-releasing factors received by neurons? A simple model is that neurons directly receive the factors released from MSCs through the interstitial space. However, machinery that bridges MSCs and neurons might facilitate more efficient transmission than direct transmission. Studies have shown that proteins and RNA can be passed from a mammalian donor cell to a target cell through gap junctions, exosomes, or tunneling nanotubules [37–39]. Direct cell contact between MSCs and neurons is also proposed. A previous study [25] suggested that few bone marrow-derived MSCs fused with the PCs of *Lurcher* ataxic mice and that most of these MSCs were located adjacent to the PC layer and expressed brain-derived neurotrophic factor (BDNF), neurotrophin-3 (NT-3), or glial cell-derived neurotrophic factor (GDNF); all of these neurotrophic factors are implicated in PC survival [25]. Thus, a major therapeutic pathway caused by MSCs may be that administered MSCs are attracted by degenerating neurons, make contact with the neurons, and directly provide neurotrophic factors to those cells to rescue them from degeneration. In line with the observation above, our preliminary experiment also showed that GFP-labeled MSCs directly injected into the cerebellar cortex of SCA1-Tg mice located in close proximity to PC somata. Thus, degenerating neurons might receive the factors from interstitial space or through special machinery such as gap junctions, exosomes, tunneling nanotubules, and cell fusion (Fig. 2).

In addition to release of innate MSC factors described above, human MSCs are excellent in vivo delivery vehicles for enzymes and proteins, as the cell type to produce and convey RNA interference (RNAi) [35, 40]. For example, experiments have been conducted with an MSC-based platform to produce and deliver RNAi moieties targeted to huntingtin mRNA as a potential therapeutic avenue for treating Huntington's disease [41].

Application of MSCs to SCA Patients

MSCs represent a promising tool in cell therapy and are currently being tested in FDA-approved phase I–III clinical trials for many disorders [30]. The cases of nervous system diseases that have received intrathecal injections of MSCs are accumulating. Regarding neuronal diseases other than SCA, MSC therapy can improve/stabilize the course of progressive

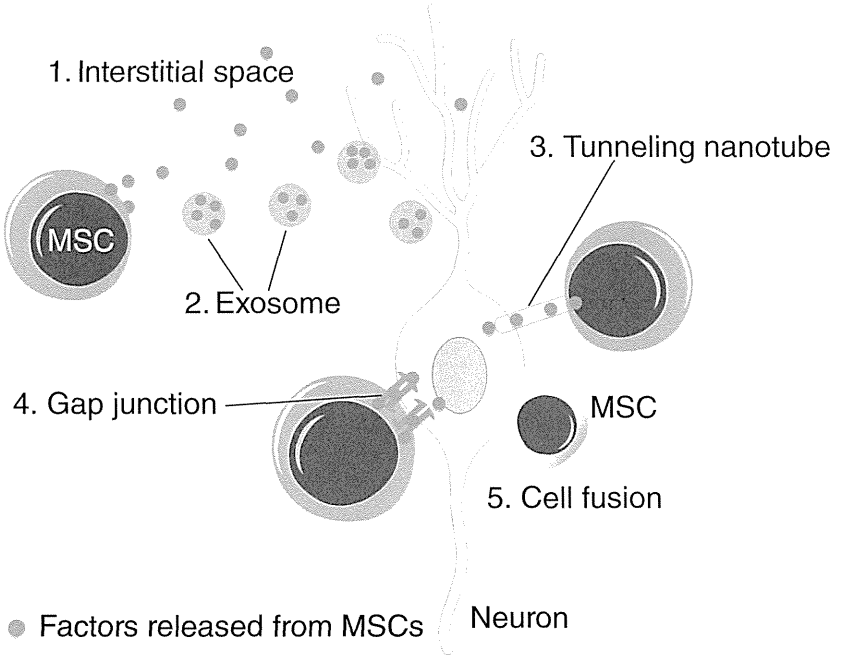

Fig. 2 Possible pathways for the transfer of factors from MSCs to neurons. Injected MSCs are likely attracted by degenerating neurons, make contact with the neurons, and directly provide neurotrophic factors to those cells to rescue them from degeneration. Neurons might receive the factors directly through the interstitial space (*1*) or via a special machinery such as exosomes (*2*), tunneling nanotubules (*3*), gap junctions (*4*), and cell fusion (*5*)

multiple sclerosis in the first year after injection, with no serious adverse effects [29]. In addition, umbilical cord MSC injections into patients with spinal cord injuries were effective in 13 of 22 patients [42]. In most patients for whom treatment was effective, motor functions, sensory functions, or both were improved along with bowel and bladder control abilities. However, minor populations experienced headache (one case) or lower back pain (one case) during the intrathecal injection, although no treatment-related adverse events occurred during a follow-up period that ranged from 3 months to 3 years [42].

Umbilical cord MSCs are also used for SCA patients. Fourteen cases of SCA patients were given an intrathecal injection of umbilical cord MSCs [43]. The intrathecal injection of umbilical cord MSCs could delay the progression of neurologic deficits for SCA. When the movement ability and quality of daily life were evaluated using the International Cooperative Ataxia Rating Scale (ICARS) and Activity of Daily Living (ADL) Scale, the ICARS and ADL scores were significantly decreased 1 month after the treatment.

In another study using umbilical cord MSCs for SCA patients, 16 genomically diagnosed SCA patients including SCA1, SCA2, and SCA3 received intravenous and intrathecal infusion of umbilical cord MSCs [44]. The laboratory examinations demonstrated that the umbilical cord MSC therapy was safe. Additionally, the majority of patients showed improved scores on the Berg Balance Scale (BBS) and ICARS, which continued for at least 6 months. Collectively, it seems that umbilical cord MSCs improve the movement ability and quality of daily life in the absence of serious side effects.

Conclusions

MSCs, multi-potent progenitor cells, can easily be isolated from multiple sources [21–23] and do not show serious adverse events or rejection reactions [31, 32]. Furthermore, MSCs shield themselves from the immune system [33], which enables their transplantation without an exact tissue match. Human MSCs are known to secrete a variety of growth factors that exert both paracrine and autocrine activities on the damaged brain tissues [34]. The effects are diverse, including the suppression of local inflammation; enhancement of angiogenesis; reduction of free radical levels; inhibition of fibrosis and apoptosis; and stimulation of the recruitment, retention, proliferation, and differentiation of tissue-residing stem cells [35]. Notably, umbilical cord MSCs seem to improve the movement ability and quality of daily life [43, 44]. Determination of the optimal protocol for MSC transplantation that maximizes therapeutic benefits and minimizes adverse reactions will be explored in the future.

Conflict of Interest There are no potential conflicts of interest in the content of this paper.

References

1. Orr HT. Cell biology of spinocerebellar ataxia. J Cell Biol. 2012;197:167–77.
2. Manto MU. The wide spectrum of spinocerebellar ataxias (SCAs). Cerebellum. 2005;4:2–6.
3. Taroni F, DiDonato S. Pathways to motor incoordination: the inherited ataxias. Nat Rev Neurosci. 2004;5:641–55.
4. Matilla-Duenas A, Goold R, Giunti P. Clinical, genetic, molecular, and pathophysiological insights into spinocerebellar ataxia type 1. Cerebellum. 2008;7:106–14.
5. Robitaille Y, Schut L, Kish SJ. Structural and immunocytochemical features of olivopontocerebellar atrophy caused by the spinocerebellar ataxia type 1 (SCA-1) mutation define a unique phenotype. Acta Neuropathol. 1995;90:572–81.
6. Harding AE. Classification of the hereditary ataxias and paraplegias. Lancet. 1983;1:1151–5.
7. Burright EN, Clark HB, Servadio A, Matilla T, Feddersen RM, Yunis WS, et al. SCA1 transgenic mice: a model for neurodegeneration caused by an expanded CAG trinucleotide repeat. Cell. 1995;82:937–48.
8. Clark HB, Burright EN, Yunis WS, Larson S, Wilcox C, Hartman B, et al. Purkinje cell expression of a mutant allele of SCA1 in transgenic mice leads to disparate effects on motor behaviors, followed by a progressive cerebellar dysfunction and histological alterations. J Neurosci. 1997;17:7385–95.
9. Xia H, Mao Q, Eliason SL, Harper SQ, Martins IH, Orr HT, et al. RNAi suppresses polyglutamine-induced neurodegeneration in a model of spinocerebellar ataxia. Nat Med. 2004;10:816–20.
10. Lee Y, Samaco RC, Gatchel JR, Thaller C, Orr HT, Zoghbi HY. miR-19, miR-101 and miR-130 co-regulate ATXN1 levels to potentially modulate SCA1 pathogenesis. Nat Neurosci. 2008;11:1137–9.
11. Hirai H. Progress in transduction of cerebellar Purkinje cells in vivo using viral vectors. Cerebellum. 2008;7:273–8.
12. Sawada Y, Kajiwara G, Iizuka A, Takayama K, Shuvaev AN, Koyama C, et al. High transgene expression by lentiviral vectors causes maldevelopment of Purkinje cells in vivo. Cerebellum. 2010;9:291–302.
13. Torashima T, Koyama C, Iizuka A, Mitsumura K, Takayama K, Yanagi S, et al. Lentivector-mediated rescue from cerebellar ataxia in a mouse model of spinocerebellar ataxia. EMBO Rep. 2008;9:393–9.
14. Chintawar S, Hourez R, Ravella A, Gall D, Orduz D, Rai M, et al. Grafting neural precursor cells promotes functional recovery in an SCA1 mouse model. J Neurosci. 2009;29:13126–35.
15. Mazzini L, Ferrero I, Luparello V, Rustichelli D, Gunetti M, Mareschi K, et al. Mesenchymal stem cell transplantation in amyotrophic lateral sclerosis: a phase I clinical trial. Exp Neurol. 2010;223:229–37.
16. Chen J, Li Y, Katakowski M, Chen X, Wang L, Lu D, et al. Intravenous bone marrow stromal cell therapy reduces apoptosis and promotes endogenous cell proliferation after stroke in female rat. J Neurosci Res. 2003;73:778–86.
17. Li Y, Chen J, Zhang CL, Wang L, Lu D, Katakowski M, et al. Gliosis and brain remodeling after treatment of stroke in rats with marrow stromal cells. Glia. 2005;49:407–17.
18. Lagasse E, Connors H, Al-Dhalimy M, Reitsma M, Dohse M, Osborne L, et al. Purified hematopoietic stem cells can differentiate into hepatocytes in vivo. Nat Med. 2000;6:1229–34.

19. Pittenger MF, Mackay AM, Beck SC, Jaiswal RK, Douglas R, Mosca JD, et al. Multilineage potential of adult human mesenchymal stem cells. Science. 1999;284:143–7.
20. Woodbury D, Reynolds K, Black IB. Adult bone marrow stromal stem cells express germline, ectodermal, endodermal, and mesodermal genes prior to neurogenesis. J Neurosci Res. 2002;69:908–17.
21. Baddoo M, Hill K, Wilkinson R, Gaupp D, Hughes C, Kopen GC, et al. Characterization of mesenchymal stem cells isolated from murine bone marrow by negative selection. J Cell Biochem. 2003;89:1235–49.
22. Gimble J, Guilak F. Adipose-derived adult stem cells: isolation, characterization, and differentiation potential. Cytotherapy. 2003;5: 362–9.
23. Lee OK, Kuo TK, Chen WM, Lee KD, Hsieh SL, Chen TH. Isolation of multipotent mesenchymal stem cells from umbilical cord blood. Blood. 2004;103:1669–75.
24. Paul G, Anisimov SV. The secretome of mesenchymal stem cells: potential implications for neuroregeneration. Biochimie. 2013;95: 2246–56.
25. Jones J, Jaramillo-Merchan J, Bueno C, Pastor D, Viso-Leon M, Martinez S. Mesenchymal stem cells rescue Purkinje cells and improve motor functions in a mouse model of cerebellar ataxia. Neurobiol Dis. 2010;40:415–23.
26. Zuo J, De Jager PL, Takahashi KA, Jiang W, Linden DJ, Heintz N. Neurodegeneration in Lurcher mice caused by mutation in delta2 glutamate receptor gene. Nature. 1997;388:769–73.
27. Matsuura S, Shuvaev AN, Iizuka A, Nakamura K, Hirai H. Mesenchymal stem cells ameliorate cerebellar pathology in a mouse model of spinocerebellar ataxia type 1. Cerebellum. 2014;13:323–30.
28. Zhang MJ, Sun JJ, Qian L, Liu Z, Zhang Z, Cao W, et al. Human umbilical mesenchymal stem cells enhance the expression of neurotrophic factors and protect ataxic mice. Brain Res. 2011;1402:122–31.
29. Bonab MM, Sahraian MA, Aghsaie A, Karvigh SA, Hosseinian SM, Nikbin B, et al. Autologous mesenchymal stem cell therapy in progressive multiple sclerosis: an open label study. Curr Stem Cell Res Ther. 2012;7:407–14.
30. Olson SD, Pollock K, Kambal A, Cary W, Mitchell GM, Tempkin J, et al. Genetically engineered mesenchymal stem cells as a proposed therapeutic for Huntington's disease. Mol Neurobiol. 2012;45:87–98.
31. Hare JM, Traverse JH, Henry TD, Dib N, Strumpf RK, Schulman SP, et al. A randomized, double-blind, placebo-controlled, dose-escalation study of intravenous adult human mesenchymal stem cells (prochymal) after acute myocardial infarction. J Am Coll Cardiol. 2009;54:2277–86.
32. Newman RE, Yoo D, LeRoux MA, Danilkovitch-Miagkova A. Treatment of inflammatory diseases with mesenchymal stem cells. Inflamm Allergy Drug Targets. 2009;8:110–23.
33. Le Blanc K. Mesenchymal stromal cells: tissue repair and immune modulation. Cytotherapy. 2006;8:559–61.
34. Joyce N, Annett G, Wirthlin L, Olson S, Bauer G, Nolta JA. Mesenchymal stem cells for the treatment of neurodegenerative disease. Regen Med. 2010;5:933–46.
35. Meyerrose T, Olson S, Pontow S, Kalomoiris S, Jung Y, Annett G, et al. Mesenchymal stem cells for the sustained in vivo delivery of bioactive factors. Adv Drug Deliv Rev. 2010;62:1167–74.
36. Aizman I, Tate CC, McGrogan M, Case CC. Extracellular matrix produced by bone marrow stromal cells and by their derivative, SB623 cells, supports neural cell growth. J Neurosci Res. 2009;87: 3198–206.
37. Gahan PB, Stroun M. The virtosome—a novel cytosolic informative entity and intercellular messenger. Cell Biochem Funct. 2010;28: 529–38.
38. Gerdes HH, Carvalho RN. Intercellular transfer mediated by tunneling nanotubes. Curr Opin Cell Biol. 2008;20:470–5.
39. Simons M, Raposo G. Exosomes—vesicular carriers for intercellular communication. Curr Opin Cell Biol. 2009;21:575–81.
40. Meyerrose TE, Roberts M, Ohlemiller KK, Vogler CA, Wirthlin L, Nolta JA, et al. Lentiviral-transduced human mesenchymal stem cells persistently express therapeutic levels of enzyme in a xenotransplantation model of human disease. Stem Cells. 2008;26:1713–22.
41. Olson SD, Kambal A, Pollock K, Mitchell GM, Stewart H, Kalomoiris S, et al. Examination of mesenchymal stem cell-mediated RNAi transfer to Huntington's disease affected neuronal cells for reduction of huntingtin. Mol Cell Neurosci. 2012;49:271–81.
42. Liu J, Han D, Wang Z, Xue M, Zhu L, Yan H, et al. Clinical analysis of the treatment of spinal cord injury with umbilical cord mesenchymal stem cells. Cytotherapy. 2013;15:185–91.
43. Dongmei H, Jing L, Mei X, Ling Z, Hongmin Y, Zhidong W, et al. Clinical analysis of the treatment of spinocerebellar ataxia and multiple system atrophy-cerebellar type with umbilical cord mesenchymal stromal cells. Cytotherapy. 2011;13:913–7.
44. Jin JL, Liu Z, Lu ZJ, Guan DN, Wang C, Chen ZB, et al. Safety and efficacy of umbilical cord mesenchymal stem cell therapy in hereditary spinocerebellar ataxia. Curr Neurovasc Res. 2013;10:11–20.